Title:

A tripartite flip-flop sleep circuit switches sleep states

Authors: Elisabeth Maluck†, Inka Busack†, Judith Besseling, Florentin Masurat, Michal Turek, Henrik Bringmann*

Affiliations:

Max Planck Institute for Biophysical Chemistry, Am Fassberg 11, 37077 Göttingen, Germany

University of Marburg, Karl-von-Frisch-Str. 8, 35043 Marburg, Germany

*correspondence to: Henrik.Bringmann@mpibpc.mpg.de

†these authors contributed equally

Abstract

Inhibitory sleep-active neurons depolarize at sleep onset to shut down the activity of wakefulness circuits. Wake-active arousal neurons in turn suppress inhibitory sleep-active neurons, thus forming a bipartite flip-flop switch. However, how sleep states are switched is unclear because neural circuits that directly depolarize inhibitory sleep-active neurons are not understood. Using optogenetics, we solved the presynaptic circuit for depolarization of the sleep-active RIS neuron in *C. elegans.* Surprisingly, we found that the PVC forward command interneuron, which is known to control wake behavior, is a major activator of RIS. The PVCs are inhibited by reverse command interneurons, which are stimulated by arousing cues. This suggests a model for sleep switch operation in which declining arousal increases activation of PVC, thus triggering activation of RIS. Depolarization of RIS in turn promotes the activation of PVC, thus forming a positive feedback loop for all-or-none sleep induction. The flip-flop sleep switch in *C. elegans* thus is tripartite and requires excitatory sleep-promoting neurons activated by wakefulness that act as an amplifier that translates reduced arousal into the depolarization of an inhibitory sleep-active neuron. A tripartite flip-flop switch likely also underlies sleep state switching in other animals including in mammals.

Introduction

Sleep is a behavior that affects many, if not all, physiological processes. Disorders and curtailment of sleep affect the lives of 10-30% of the adult population of modern societies. Sleep deprivation is detrimental to human health and is associated with an increased risk of infection, cardiovascular disease, depression, obesity, type 2 diabetes, and cancer. The high prevalence of insomnia and insufficient sleep quality thus presents a massive unmet health and economic problem[1-4]. To understand how behavior is generated, it is crucial to solve the underlying neural circuits. For example, the circuit of the crustacean stomatogastric nervous system showed that neuromodulation alters behavior without changing the connectome[5], the learning circuits in *Aplysia* revealed synaptic mechanisms of memory formation[6], and the grid cell circuit in the mammalian entorhinal cortex demonstrated how a map of the spatial environment can be encoded[7].

Sleep circuits require inhibitory sleep-active sleep-promoting neurons, which depolarize specifically at sleep onset and actively induce sleep by releasing inhibitory neurotransmitters, GABA and neuropeptides, to dampen arousal and the activity of wake circuits[8]. The depolarization of inhibitory sleep-active neurons defines the key properties of sleep behavior, which are the suppression of voluntary movements and sensory perception, reversibility, and homeostasis[9]. Inhibitory sleep-active neurons suppress wake circuits leading to a reduction of voluntary movement, sensory processing, and reduced responsiveness to stimulation. Inhibitory sleep-active neurons can be rapidly suppressed by arousing stimulation to allow for quick awakening. Forced wakefulness is followed by an increase of inhibitory sleep-active neuron depolarization, which leads to homeostatic sleep corrections. Thus, understanding sleep control requires comprehension of the circuit mechanisms that determine when and how much inhibitory sleep-active neurons depolarize[8, 10].

Circuits control the depolarization of inhibitory sleep-active neurons. For example, wake-active wake-promoting neurons promote arousal and suppress inhibitory sleep-active neurons, whereas sleep need causes tiredness and inhibitory sleep-active neuron

depolarization. Thus, inhibitory sleep-active sleep-promoting and wake-active wake-promoting neurons form a flip-flop switch, which ensures that sleep and wake exist as discrete states. This sleep switch is under the control of arousal that favors wake and inhibits sleep through the suppression of sleep-active neurons by inhibitory wake-active neurons[8, 11]. It has been proposed that sleep induction is favored by disinhibition of inhibitory sleep-active neurons [12-14], and also excitatory sleep-active neurons exist that might perhaps present activators of inhibitory sleep-active neurons [15]. However, the forces and mechanisms that flip the sleep switch from wake to sleep when an organism gets tired cannot be satisfactorily explained by the present circuit models as it is unclear how inhibitory sleep-active neurons are turned on when the system is set to sleep.

Sleep is under circadian and homeostatic controls that determine the timing of sleep and ensure that enough of this essential physiological state takes place[16]. Sleep homeostasis comprises multiple mechanisms that act on different time scales. On long time scales sleep is a function of prior wakefulness, i.e. prolonged wakefulness leads to increased sleep propensity and sleep loss triggers compensatory increases in the intensity or duration of sleep. This chronic sleep homeostasis likely is mediated by several parallel mechanisms. For example, in mammals, somnogens such as adenosine accumulate during wakefulness leading to the inhibition of wake-promoting neurons[17, 18]. In *Drosophila*, activity-dependent plasticity of sleep-promoting neurons increases during wakefulness to increase subsequent sleep[19, 20]. On short time scales, acute homeostasis determines whether the system's actual state matches the system's set point and carries out corrective action if those values do not match. For example, to homeostatically maintain sleep despite disturbance, micro arousals need to be compensated for. In humans, homeostatic sleep maintenance can be seen in EEG recordings in the form of k-complexes, where a spontaneous or evoked short cortical up state is followed by a down state[21-23]. Homeostatic sleep maintenance is also found during sleep in *C. elegans,* where sleep bouts are interrupted by short motion bouts, with the length of a motion bout correlating with the length of the subsequent sleep bout[24, 25]. Thus, across systems, homeostatic sleep maintenance requires constant surveillance of sleep and corrective action.

Sleep-active sleep-promoting neurons are conserved regulators of sleep and have been found both in vertebrates as well as in invertebrates[10, 26]. Mammals possess several populations of sleep-active neurons across the brain, most of which are inhibitory, including neurons in the anterior hypothalamus, brain stem, and cortex [8, 14]. Excitatory sleep-active neurons were found in the periocular midbrain that project to inhibitory sleep-active neurons in the anterior hypothalamus, whose role could be to activate inhibitory sleep-active neurons, but this hypothesis has yet to be tested experimentally[15]. Studying sleep in less complex brains facilitates sleep circuit analysis. In *Drosophila*, sleep-promoting neurons are found at several locations in the brain. A well-characterized population of sleep-promoting neurons is formed by ExFl1 neurons residing in the dorsal fan-shaped body. R2 neurons accumulate homeostatic sleep pressure over time to promote activation of ExFl1 neurons, probably by an indirect mechanism [19, 20]. *C. elegans* possesses a single inhibitory sleep-active neuron called RIS. Like its mammalian counterparts, RIS depolarizes at sleep onset. RIS is crucial for sleep induction as its ablation leads to a virtually complete loss of detectable sleep bouts[27-29]. The small, invariant nervous system, its mapped connectome, and the transparency of *C. elegans* facilitates neural circuit analysis[30]. However, the specific neural circuits that control RIS activity are not yet understood.

C. elegans shows sleep behavior during many stages and conditions. Here we analyzed sleep behavior during lethargus, the stage prior to each of the four molts during larval development [10, 29, 31-33]. We used optogenetics to dissect the neural circuit that controls the activation of the inhibitory sleep-active RIS neuron in *C. elegans*. We found that the PVC command interneurons, which are activated by wakefulness, are sleep-promoting by turning on the RIS sleep-active neuron. PVC activity is inhibited by reverse arousal command interneurons that thus inhibit sleep. This tripartite flip-flop circuit can explain how arousing stimulation inhibits RIS depolarization, how RIS depolarization is homeostatically controlled, and how reduced arousal can induce RIS depolarization.

Results

130 **A command interneuron circuit controls RIS activity**

131

132 RIS is crucially required for sleep and activates during each sleep bout (Figure 1A) [27].
133 However, the presynaptic driver neurons that activate and control this neuron are not
134 known. To identify the circuits controlling RIS activation transients, we optogenetically
135 tested the role of neurons that are presynaptic to RIS according to the *C. elegans*
136 connectome [30]. The neurons AVJL, CEPDL, URYVL, RIMR, PVCL, and SDQL have
137 been shown to be presynaptic to RIS[30]. To find out how these presynaptic neurons
138 control RIS, we activated them with ReaChR and green light, and followed RIS calcium
139 activity during and outside of lethargus. Because there were no specific promotors
140 available for the expression in SDQL and PVC, we expressed ReaChR using semi-specific
141 promoters and selectively illuminated only the presynaptic neuron class. We used L1 larvae
142 for most of the optogenetic experiments to dissect the circuit. As SDQL is born
143 postembryonically and likely is not yet functional during the L1 stage, we used L4 larvae
144 to assay its function[34]. We compared the effects of optogenetic stimulation outside and
145 during lethargus, defined as the period prior to the molt during which the animals do not
146 feed[35]. Before lethargus, we measured an activation of RIS upon depolarization of AVJ,
147 CEP and SDQL, whereas activation of the other neurons tested caused no significant
148 change in RIS activity. During lethargus, the activation of CEP, PVC and SDQL caused
149 RIS activation (Figure 1B, Supplementary Figure 1A). All neurons showed consistent
150 effects on RIS depolarization except RIM. While RIM caused only a minor and non-
151 significant net activation of RIS in the averaged measurements, RIM activation either
152 activated or inhibited RIS depending on the trial (Figure S1B-C).

153

154 PVC appeared to be a strong activator of RIS only during lethargus. This suggested that
155 either the PVC to RIS connection might be specific for lethargus or that it has not yet
156 matured during the mid L1 stage. We hence repeated the experiment and activated PVC in
157 L2 larvae. PVC activated RIS both during and outside of lethargus, but the activation
158 during lethargus was much stronger, suggesting that the activation of RIS by PVC is
159 strongly enhanced during lethargus (Figure S1C). To find out which presynaptic neurons
160 are required for inhibition or activation of RIS during lethargus, we tested the effect of

161 optogenetic inhibition of the presynaptic neurons on RIS activation. We used ArchT, which
162 hyperpolarizes neurons by pumping protons out of the cell [36, 37]. As before, we
163 specifically illuminated each presynaptic neuron class and quantified RIS activation using
164 calcium imaging. Before lethargus, inhibition of AVJ and PVC led to an inhibition of RIS,
165 whereas inhibition of the other neurons tested had no acute significant effect on RIS.
166 During lethargus, only optogenetic inhibition of PVC led to significant RIS inhibition,
167 whereas there was no effect seen for the other neurons (Figure 1C, Figure S2A). While
168 inhibition of RIM had no significant net effect on RIS, in roughly one quarter of the
169 measured trials, the inhibition of RIM led to RIS inhibition before and during lethargus
170 (Figure S2B).
171
172 Our optogenetic analysis revealed a complex set of presynaptic inputs for regulation of RIS
173 activity. The optogenetic gain-of-function experiments suggest that CEP, PVC, and SDQL
174 present the most potent presynaptic activators of RIS. The capacity of PVC to activate RIS
175 is strongly increased during lethargus, indicating that this neuron is involved in the
176 lethargus-specific activation of RIS. The optogenetic loss-of-function experiments suggest
177 that PVC is an essential presynaptic activator of RIS during lethargus, but additional
178 neurons might contribute to RIS activation during lethargus or other conditions. RIM has
179 the potential to both inhibit and activate RIS. While the activation could be direct, RIM is
180 known to be an inhibitor of PVC through activation of the reverse command interneurons
181 AVA/AVD/AVE and could thus perhaps inhibit RIS indirectly [38-40]. Consistent with
182 the lack of net effects of RIM on RIS, RIM ablation does not change spontaneous sleep
183 amounts (Figure S2C). Therefore, the majority of synaptic inputs into RIS is activating and
184 inhibition appears to be predominantly indirect. The CEP, URY, and SDQL neurons
185 present sensory receptors and might play a role in activating RIS in response to stimulation
186 [41, 42]. Because of the strong and lethargus-specific effects of the PVC neurons on RIS
187 activation we focused our analysis on these key neurons.
188
189 As the PVC neurons are crucial activators of RIS we tested their role in inducing sleep
190 behavior. We used a strain that ablated PVC and other command interneurons by
191 expressing the pro-apoptosis regulator ICE from the *nmr-1* promotor and measured sleep

192 and RIS activation[43]. Command interneuron ablation reduced sleep bouts during
193 lethargus by about 76% (Figure S3A). The command interneuron-ablated worms also
194 generally moved much slower (Figure S3B) and RIS activation was reduced by 63%
195 (Figure S3C). Quiescence bouts did not occur at the beginning of the lethargus phase as
196 defined by cessation of feeding, and were only observed around the middle of the lethargus
197 phase (Figure S3D). An independently generated strain that ablates command interneurons
198 using *egl-1* expression caused a reduction of sleep by 81% (Figure S2A). Because the
199 command interneurons are controlled by glutamatergic signaling we also tested mutants in
200 which this type of signaling is impaired and also observed impaired sleep consistent with
201 ablating command interneurons (Figure S4).
202
203 To be able to more specifically manipulate PVC and to test the effects of PVC inhibition
204 on behavior without affecting the other command interneurons, we used a more specific
205 promoter for expression in PVC, which had been identified from single-cell RNA
206 sequencing data [44, 45](Jonathan Packer, personal communication). There was no gene
207 in the available datasets that was expressed only in the cluster of cells containing PVC, but
208 the previously uncharacterized gene *zk673.11* was expressed strongly in PVC and in only
209 a few other neurons excluding other command interneurons and therefore we used the
210 promoter of this gene for PVC expression (Figure S5). Hyperpolarization of PVC through
211 activation of ArchT led to an acute inhibition of RIS, an increase in locomotion, and a
212 reduction of sleep (Figure 1D). These experiments show that RIS is controlled by a
213 command interneuron circuit. The major command interneuron activator of RIS during L1
214 lethargus are the PVC forward command interneurons (Figure 1E). While PVC has
215 previously been shown to promote forward locomotion[46], its inhibition leads to increased
216 mobility implying that the reduction of locomotion after simultaneous ablation of most
217 command interneurons stems from the reverse command interneurons that promote
218 mobility, whereas PVC appears to play a predominant role in dampening motion behaviors
219 through activation of RIS.
220
221 **RIS and PVC activate each other forming a positive feedback loop**
222

223 PVC presents a major activator of RIS, but how a forward command interneuron can cause
224 massive activation of the RIS neuron during sleep bouts is not clear. We hence tested how
225 optogenetic RIS activation affects PVC activity. We selectively activated RIS using
226 ReaChR and measured calcium activity in PVC (Figure 2A). Because the calcium
227 transients observable in PVC are typically small we used immobilized worms to reduce
228 measurement noise[47]. Upon RIS stimulation, PVC immediately displayed unexpectedly
229 strong calcium transients, which were slightly stronger during lethargus (Figure 2B, Figure
230 S6A). These results show that PVC and RIS activate each other, thus forming a positive
231 feedback loop. The strong calcium activation of PVC by RIS depolarization is striking
232 because activation transients in PVC have hitherto only been observed after mechanical
233 stimulation, whereas spontaneous PVC activity transients have not yet been reported[47].
234 The sleep-inducing RIS neuron has so far only been shown to inhibit other neurons making
235 PVC the first neuron which is not inhibited but activated by RIS. For example, command
236 interneurons such as AVE/AVA and other neurons are not activated by RIS but
237 inhibited[27]. While PVC is presynaptic to RIS, RIS is not presynaptic to PVC. The
238 activation of PVC by RIS could involve diffusional mechanisms or could be indirect
239 through other neurons, perhaps mediated by the inhibition of a PVC inhibitor such as
240 AVA/AVD/AVE. It is currently not possible to measure spontaneous calcium transients in
241 PVC, but our results would predict that PVC should spontaneously activate during sleep
242 bouts, which would characterize PVC not only as a neuron active during wakefulness as
243 suggested by previous studies[46, 47] but also as a sleep-active neuron. It would thus differ
244 from previously identified sleep-active neurons in that it does not induce sleep directly by
245 inhibiting wake circuits but indirectly through activation of an inhibitory sleep-active
246 sleep-inducing neuron. As PVC is activated by wakefulness and also promotes sleep, it
247 would thus be ideally suited to mediate the transition from active to quiescent states.
248 Together, these data suggest that PVC and RIS rely on positive feedback to achieve strong
249 transients during a sleep bout.
250
251 If depolarization of RIS activates PVC, what consequences does hyperpolarization of RIS
252 have on PVC activity? To answer this question, we measured the response of PVC to RIS
253 inhibition. We hyperpolarized RIS optogenetically for one minute using ArchT and

254 measured the activity of PVC. Interestingly, PVC showed a small but significant activity
255 increase during RIS inhibition, an effect which was increased during lethargus (Figure 2C).
256 The disinhibition of PVC by RIS inactivation is likely not direct and may reflect a general
257 increase in neuronal and behavioral activity that is caused by RIS inhibition and that
258 extends to the PVC neurons. Since PVC is a major activator of RIS, its disinhibition could
259 be part of a homeostatic feedback regulation.
260
261 Our results suggest that there is a positive feedback from sleep induction onto RIS
262 activation and that full RIS activation is only possible when sleep is successfully induced,
263 explaining the strong correlation of RIS depolarization and sleep bout induction[29]. This
264 model would predict that RIS transients are dampened if RIS is not able to induce sleep
265 bouts. To test this idea we analyzed RIS calcium transients in *aptf-1(-)* mutant worms in
266 which RIS still shows depolarization transients during lethargus, but cannot efficiently
267 induce quiescence behavior because its inhibitory neuropeptides are not expressed[27, 48].
268 In *aptf-1(-)* mutant animals, calcium transients' maxima were reduced by about 35%
269 (Figure 2 D-E). These results are consistent with the idea that sleep induction is a self-
270 enforcing process in which RIS-mediated inhibition of brain activity promotes further RIS
271 activation (Figure 2F).
272
273 **RIS depolarization is under homeostatic control**
274
275 The design of the sleep circuit suggests an intimate mutual control mechanism of RIS and
276 command interneurons that could allow homeostatic control of sleep. Arousing stimulation
277 is known to inhibit sleep-active neurons and to increase subsequent sleep[24, 25, 27, 29].
278 We thus hypothesized that inhibition of RIS leads to its subsequent depolarization, forming
279 a homeostat that allows maintaining or reinstating sleep bouts. We tested this hypothesis
280 by optogenetically hyperpolarizing RIS and following its activity using calcium imaging.
281 We inhibited RIS directly for 60 seconds by expressing the light-driven proton pump
282 ArchT specifically in this neuron and used green light illumination to activate ArchT. We
283 followed RIS calcium activity using GCaMP during the experiment and quantified
284 behavior. Optogenetic hyperpolarization of RIS led to a decrease in intracellular calcium

285 and increased behavioral activity. Approximately one minute after the end of the inhibition,
286 RIS showed a rebound activation transient during which calcium activity levels increased
287 strongly and rose well above baseline levels, concomitant with a decrease in behavioral
288 activity. Overall brain activity measurements showed that behavioral activity and brain
289 activity correlated throughout the experiment (Figure 3A). Strikingly, while the rebound
290 transient was also measurable outside of lethargus, the strength of the RIS rebound
291 depolarization was three-fold stronger during lethargus than before lethargus, indicating
292 that the propensity for RIS rebound activation is strongly increased during lethargus.
293
294 To test whether rebound activation of RIS mediates acute or chronic homeostasis, we tested
295 whether the strength of the rebound activation is a function of length of prior inhibition.
296 For this experiment we increased the length of the RIS inhibition and quantified the time
297 it took after the end of the stimulation until the rebound transient started as well as the peak
298 maximum of the rebound. After inhibiting RIS for five minutes, the rebound initiated
299 immediately after the end of the stimulation and the maximum that was reached exceeded
300 that observed after about one minute of RIS stimulation. Inhibiting RIS for ten minutes did
301 not further increase the occurrence or strength of the rebound transient. These results show
302 that RIS activation rebound transients rapidly saturate with increasing length of inhibition
303 (Figure 3B, Figure S6B-D) Thus, RIS shows a rebound activation upon inhibition that leads
304 to its own subsequent activation. A rebound activation was not only seen when RIS was
305 inhibited directly, but we also saw a reactivation of RIS after it was inhibited indirectly
306 using a blue light stimulus when the worms returned to sleep (Figure S7). The rebound
307 activation presents the translation of RIS inhibition into subsequently increased RIS
308 activity and thus sleep induction. Rebound activation of RIS does not seem to constitute a
309 chronic integrator of wake time but presents an acute homeostatic regulatory phenomenon
310 to induce, maintain, or reinstate sleep bouts.
311
312 If RIS is part of a homeostatic system and RIS inhibition triggers its subsequent activation,
313 does activation of RIS also trigger its own inhibition? To test this idea, we optogenetically
314 activated RIS and measured its activity before, during, and after the manipulation. We
315 optogenetically depolarized RIS for one minute using green light and the light-activated

316 cation channel ReaChR expressed specifically in RIS. Activity of RIS was followed using
317 calcium imaging and increased strongly during optogenetic depolarization but was also
318 reduced significantly after stimulation compared with baseline activity, indicating that RIS
319 activity also shows a negative rebound. Again, this effect was highly increased, about five-
320 fold, in worms that were in lethargus compared with worms outside of lethargus (Figure
321 3C). Thus, polarization of RIS during lethargus is under homeostatic control in both
322 directions. Hyperpolarization leads to subsequent depolarization, perhaps through a
323 reactivation of wake-active circuits that ultimately lead to the reactivation of PVC.
324 Depolarization leads to subsequent hyperpolarization, perhaps through inhibition of wake-
325 active circuits that cause PVC activation. This homeostatic regulation is highly enhanced
326 during lethargus and can thus contribute to the repetitive pattern of RIS activation and thus
327 the oscillating induction of consecutive sleep bouts[24].
328
329 **Modest dampening of brain arousal occurs upstream of RIS**
330
331 Our results demonstrate that PVC plays a major role in activating RIS involving self-
332 enforcing positive feedback, resulting in strong RIS activation and thus sleep induction.
333 RIS calcium transients during development outside of lethargus are small, whereas
334 transients are high during lethargus. What determines that RIS calcium transients are
335 limited outside of lethargus but promoted during lethargus? With other words, what tips
336 the balance that allows the self-enforcing feedback loop of PVC and RIS to set off? As an
337 important principle of command interneuron control, forward and reverse command
338 interneurons inhibit each other to allow discrete forward and reverse locomotion states.
339 The AVA/AVD/AVE/RIM interneurons initiate reverse locomotion by activating pre-
340 motor interneurons while inhibiting the forward command circuit including AVB/PVC. By
341 contrast, during forward movement reverse command interneurons are inhibited [46, 49].
342
343 Small changes in arousal and activity of the command interneurons can change the
344 equilibrium of forward and reverse command interneurons [43]. Hyperactive mutants
345 suppress sleep across species including *C. elegans* [50-52]. Many arousal cues trigger
346 backwards escape movements and inhibit RIS [27, 29, 53]. Thus, previous studies on the

347 command interneuron circuit together with our results suggest that arousal inhibits RIS
348 through inhibiting PVC. This model of RIS activation would predict that there are changes
349 during lethargus that are upstream of RIS activity that change the properties of the
350 command circuit leading to increased PVC and thus RIS activation.
351
352 We reasoned that it should be possible to measure these changes that occur in command
353 interneuron activity upstream of RIS by characterizing neural activity and behavior in *aptf-*
354 *1(-)* mutant worms. We quantified behavior and command interneuron calcium levels
355 across lethargus in *aptf-1(-)* mutant worms. Wild type animals showed successive sleep
356 bouts and a 70% reduction in locomotion speed by during lethargus. By contrast, *aptf-1(-)*
357 mutant animals almost never showed quiescence bouts (Figure 2E), but nevertheless
358 locomotion speed was decreased by 25% during the lethargus phase (Figure 4). Consistent
359 with the behavioral activity reduction, there was a significant reduction of command
360 interneuron activity during lethargus also in *aptf-1(-)* mutant animals (Figure 4, Figure S8).
361 To further characterize the neuronal changes upstream of RIS-mediated sleep induction,
362 we imaged the activity of RIM as exemplary neurons during lethargus in *aptf-1(-)* mutants.
363 In wild type animals, RIM regularly showed activation transients before lethargus but did
364 not show many transients during lethargus. RIM showed not only a change in transient
365 frequency across the lethargus cycle but also a reduction in baseline calcium activity. In
366 *aptf-1(-)* mutant worms, RIM continued showing RIS transients during lethargus,
367 indicating that RIS inhibits RIM transients during sleep bouts. However, reduction of
368 baseline calcium activity was preserved in *aptf-1(-)*, indicating that RIM activity is
369 dampened during lethargus independently of RIS at the level of baseline calcium activity.
370 Together these experiments indicate that a dampening of behavioral and neural baseline
371 activity occurs during lethargus that is independent of RIS. This neuronal baseline and
372 behavioral dampening itself appears not to be sufficient to constitute normal sleep bouts,
373 but could hypothetically lead to a weaker activity of reverse arousal neurons thus allowing
374 stronger or longer activation of forward command interneurons including PVC and thus
375 RIS activation[43, 54].
376
377 **An arousing stimulus inhibits RIS through RIM**

378

379 Arousal plays a major role in inhibiting sleep but the circuits that mediate the effect of
380 arousing stimuli on RIS inhibition are not well understood. We hence studied the circuit
381 by which stimulation of a nociceptor, the ASH neurons, leads to a reverse escape response
382 and inhibition of RIS[55]. We optogenetically stimulated ASH using ReaChR and green
383 light and followed RIS and RIM activities. ASH activation led to the activation of the RIM
384 neuron and triggered a backwards response as previously described [55, 56].
385 Simultaneously, RIS was inhibited (Figure 5A). RIM can inhibit PVC through reverse
386 interneurons which it synchronizes, making it ideally suited to mediate the effects of ASH
387 stimulation[39, 46]. To test whether RIM is required for RIS inhibition, we ablated RIM
388 genetically by expression of *egl-1* from the *tdc-1* promoter, which is specific to RIM and
389 RIC, and repeated the optogenetic stimulation of ASH. We used L4 stage animals as the
390 genetic ablation was not yet effective in L1 animals. In RIM-ablated animals, activation of
391 ASH caused the opposite effect on RIS activity. Instead of inhibiting RIS, ASH activated
392 RIS, while still increasing behavioral activity (Figure 5B). Consistent with our calcium
393 imaging data, ASH stimulation after RIM ablation predominantly caused a forward
394 locomotion response (Figure 5C). Further supporting the idea that reverse interneurons
395 inhibit and forward PVC neurons activate RIS during stimulation, gentle tail touch
396 increased RIS activity more strongly when RIM was ablated (Figure S9). These results
397 delineate a circuit model for how sensory stimulation can control RIS activation. By
398 activating the reverse response that is mediated by RIM, PVC is suppressed leading to RIS
399 inhibition. In addition, sensory stimulation can also promote RIS activation if the forward
400 command circuit is activated.

401

402 **Discussion**

403

404 **A tripartite flip-flop circuit controls sleep**

405

406 Optogenetic activation and inhibition showed how the activity of presynaptic neurons
407 affects RIS depolarization during developmental sleep. Several presynaptic neurons can
408 activate RIS, but potent direct inhibitors were not identified. Loss-of-function experiments

409 showed that the command circuit controls activation of RIS, with PVC presenting the key
410 activator of RIS. PVC has long been known to mediate the forward escape response by
411 transmitting information from posterior sensory neurons to activate AVB pre-motor
412 neurons to trigger forward locomotion[46, 47, 57]. Consistent with promoting the forward
413 escape response, optogenetic activation of PVC leads to an, albeit modest, increase in
414 forward movement[57, 58]. Reverse movement, in turn, is mediated by AVA, AVE, and
415 AVD command premotor interneurons, which activate reverse motor neurons. Forward
416 PVC and reverse AVA/AVE/AVD command interneurons are presynaptic to and mutually
417 inhibit each other, which ensures discrete forward and reverse locomotion states analogous
418 to a flip-flop switch [40, 43, 46].
419
420 Our finding that PVC presents a key activator of RIS immediately suggests a model for
421 how RIS is controlled and provides a potential mechanism for linking sleep induction to
422 decreasing arousal and for homeostatically maintaining a series of sleep bouts. According
423 to this model, during conditions of high arousal, such as during development outside of
424 lethargus, larvae are constantly awake. The command interneuron circuit cycles between
425 forward and reverse states, leading to the activation of forward or reverse motor programs,
426 respectively[40, 46, 59]. Arousal promotes reverse command interneurons activity and thus
427 limits PVC and RIS activation. Independently of RIS, lethargus induces a modest neural
428 dampening that includes command interneuron activity that is evident as a decrease in
429 baseline calcium activity and reduction of locomotion speed. Consistent with the view that
430 reduction of neuronal activity can occur partially independently of RIS, the dampening of
431 sensory neurons during lethargus is not fully reversible upon stimulation[60, 61]. This
432 modest but broad activity dampening could cause a modest shift of command interneuron
433 activity that should lead to a modest favoring of PVC activity, perhaps through
434 disinhibition. Consistent with this model, sleep bouts are typically induced from long
435 forward movement bouts or periods of reduced locomotion activity and not from reverse
436 movements [54, 59, 62]. Mutations that increase arousal and suppress sleep increase the
437 activity of reversal neurons, whereas conditions that decrease arousal decrease the activity
438 of the reversal neurons and increase sleep[40, 51, 52]. Also, the ablation of reverse
439 command interneurons such as AVE reduces reversals and leads to ectopic quiescence[47,

440 63]. The increased activation of PVC in turn depolarizes RIS. Because PVC and RIS form
441 a self-reinforcing positive feedback loop, a modest increase of PVC activity could translate
442 non-linearly to a strong activation of RIS, which in turn induces the shutdown of behavior
443 that is required for the sleep state [24, 31, 54, 60, 61]. The activation of RIS leads to the
444 secretion of inhibitory neuropeptides that inhibit key arousal neurons[27, 48]. While PVC
445 is presynaptic to RIS and likely activates it directly, RIS is not presynaptic to PVC,
446 suggesting an indirect mechanism that perhaps could involve inhibition of reverse
447 command interneurons including AVA/AVE, which are inhibited by RIS [27] and could
448 thus lead to further activation of PVC through disinhibition. Thus, the process of sleep
449 induction, once it reaches a critical threshold, could become self-enforcing. In summary,
450 our model allows a circuit understanding of the mutual control of the wake-active central
451 pattern generator formed by the command interneurons and the sleep-active RIS neuron
452 and provides the mechanistic basis for understanding the correlation of sleep and
453 locomotion patterns observed in pan-neuronal imaging studies[54, 62]. Our model suggests
454 that the sleep switch is tripartite and includes self-enforcing inhibitory sleep-active sleep-
455 promoting neurons as well as excitatory wake-activated sleep-promoting neurons as
456 mediators of switch flipping. This sleep switch acts as an amplifier that can translate a
457 modest reduction of arousal into a massive shutdown of behavioral activity during sleep.
458 Dampening of neural activity independently of sleep-active neurons could be interpreted
459 as a neural equivalent of tiredness that leads to an increased propensity to activate sleep-
460 active neurons and to induce sleep bouts. Thus, the sleep switch could present an amplifier
461 that translates reduced brain activity into sleep bouts (Figure 6). Further experiments will
462 be necessary to find out how PVC activity is controlled by sleep-promoting signals such
463 as reduced arousal.
464
465 What causes the termination of sleep bouts? The PVC and RIS neurons might not be able
466 to sustain prolonged activity leading to the cessation of a sleep bout. The RIS activation
467 transient and thus sleep bout can be blunted by a sensory or optogenetic arousing stimulus
468 [27, 29, 54, 61]. Arousing stimulation, for instance by activating the nociceptive sensory
469 neurons, triggers a reverse escape response through backwards command and RIM
470 interneurons [39, 56, 59, 64]. Optogenetic RIM depolarization variably causes activation

471 or inhibition of RIS but the cause of this probabilistic outcome is unclear. Potentially, the
472 activating effect of RIM on RIS could be mediated by direct synaptic innervation and might
473 serve a buffering or probabilistic function [39], consistent with the almost zero net effects
474 of RIM depolarization on RIS activity. However, stimulation of the nociceptive ASH
475 neurons causes consistent inhibition of RIS that depends on RIM, suggesting that a main
476 physiological role of RIM is to inhibit sleep upon arousing stimulation, perhaps by
477 synchronizing the reverse interneurons[39]. RIM activation can inhibit sleep also in
478 response to acute food deprivation [65, 66]. Thus, RIM might present an arousal module
479 that can be activated upon sensing various external conditions that signal the need to
480 suppress sleep (Figure 6).
481
482 RIS inactivation leads to disinhibition of arousal and brain activity starting anew the cycle
483 of command interneuron activity and locomotion behavior. Depending on the arousal
484 levels, PVC activity should increase either immediately or after a delay until it reaches a
485 critical level sufficient to cause substantial RIS reactivation and thus a return to sleep. The
486 timing at which the rebound activation occurs can be controlled by the level of arousal,
487 with strong arousal leading to longer wake periods before the return to sleep, whereas
488 milder stimulations cause the immediate return to sleep[25]. Consistent with this circuit
489 model of recurrent RIS activation, RIS activity oscillates, resulting in the typical pattern of
490 sleep bouts that are interrupted by activity bouts[24]. This circuit design allows
491 homeostatic sleep maintenance of a series of consecutive sleep bouts with sensory
492 stimulation restarting the cycle of RIS activation thus prompting an acutely increased RIS
493 activation causing the return to sleep (Figure 6A)[25, 54].
494
495 How can PVC mediate seemingly contrary behaviors, the forward escape response and
496 sleep bout induction? Sensory mechanical stimulation causes general arousal. For example,
497 tail touch not only activates the forward PVC neurons to trigger a forward locomotion
498 response, but also activates the reverse AVA neurons, with a net dominance of the PVC
499 activation [46, 57]. Because the reverse command interneurons inhibit the forward
500 interneurons, the sensory stimulation should lead to only a limited activation of PVC that
501 is sufficient to trigger a forward movement, but that is insufficient to cause strong RIS

502 activation and thus a sleep bout. Consistent with this idea, weakening of the reverse circuit
503 by RIM ablation changes the behavioral response of tail touch during lethargus, and PVC
504 activation outside of lethargus only causes a modest increase in forward movement[57,
505 58]. During normal waking behavior, modest RIS activation may thus function to dampen
506 the behavioral response to sensory stimulation and to regulate the speed of locomotion [67,
507 68].
508
509 Here we have identified a circuit controlling sleep-active neuron depolarization in *C.*
510 *elegans*. This work built on the neural connectome and was facilitated by the small size
511 and invariance of the nervous system as well as the transparency of the organism. While
512 the *C. elegans* sleep circuit clearly is built from less cells than the human sleep circuit,
513 there are many conceptual similarities. For instance, in both *C. elegans* and humans, sleep
514 is controlled by inhibitory sleep-active sleep-promoting neurons that depolarize at sleep
515 onset to actively induce sleep by inhibiting wake circuits. A main difference is that humans
516 have many brain centers each consisting of thousands of sleep-active neurons[14]. The
517 single RIS neuron is the major inhibitory sleep-active neuron required for sleep induction
518 in *C. elegans*[27]. Work in mammals revealed the general principles of wake-active wake-
519 promoting neurons and sleep-active sleep-promoting neurons as well as their mutual
520 inhibition. While this information explains the flip-flop nature of sleep and wake states,
521 there is no satisfactory understanding of what flips the sleep switch, i.e. how wakefulness
522 is detected when the system is set to sleep, prompting the activation of inhibitory sleep-
523 active neurons [8]. Our model for the operation of the *C. elegans* sleep circuit indicates
524 that flipping of the sleep switch can be understood if excitatory wakefulness-activated
525 sleep-promoting neurons and a positive feedback of sleep-active neuron depolarization are
526 added to the switch model. In this tripartite flip-flop sleep switch model, the sleep-active
527 sleep-promoting center is activated by an excitatory sleep-promoting center that is
528 activated by wakefulness. Wake-activated sleep-promoting neurons and wake-active
529 wake-promoting neurons inhibit each other thus forming the actual flip-flop switch.
530 Arousing stimulation increases the activity of the wake-active wake-promoting neurons
531 and thus suppresses excitatory wake-activated sleep-promoting neurons and thus sleep.
532 According to this model, reducing arousal increases the activity of excitatory wake-

activated, sleep-promoting neurons and thus favors inhibitory sleep-active sleep-promoting neuron depolarization, causing sleep behavior (Figure 6). Therefore, reduced arousal and activity of wake-active wake-promoting neurons could present a neural correlate of tiredness. Excitatory neurons in the periocular midbrain of mammals are similar to PVC in that they may be activators of inhibitory sleep-active neurons an could perhaps be part of circuits that operate by mechanisms analogous to the tripartite sleep switch of *C. elegans* [15].

Sleep is reversible by stimulation and hyperarousal is the major cause for insomnia in humans[2, 69, 70]. Homeostatic sleep maintenance is an essential feature of sleep and is found from worms to humans[21-23, 25]. R2 ring neurons in *Drosophila* present an integrator of wake time causing subsequently increased depolarization of ExFl1 sleep-inducing neurons, thus forming a chronic sleep homeostat [71, 72]. Our model of a tripartite flip-flop circuit suggests that excitatory wake-activated sleep-promoting neurons are part of an acute sleep homeostat that translates acute brain activity into increased sleep neuron activity when the system is set to sleep. Excitatory wake-activated sleep-promoting neurons measure systemic activity, i.e. they become active as a consequence of a global brain activity increase, and directly activate the inhibitory sleep-active neuron transiently. Thus, the interplay of inhibitory sleep-active sleep-promoting and excitatory wake-active sleep-promoting neurons form an oscillator that periodically sends out sleep-inducing pulses. Macroscopically, sleep in mammals exists as cortical oscillations of global down states, known as slow waves[73]. Micro arousals trigger cortical upstates that are followed by cortical down states, known as k-complexes[21-23]. Both slow wave activity as well as k-complexes could be hypothetically explained by the concept of excitatory wake-activated sleep-promoting circuits.

Acknowledgments

We are grateful to Jonathan Packer and Robert Waterson for suggesting the use of the *zk673.11* promoter. We thank Andres Mariqc and Yun Zhang for strains. Some strains were provided by the CGC, which is funded by NIH Office of Research Infrastructure Programs

(P40 OD010440). This work was funded by the Max Planck Society (Max Planck Research Group), a European Research Council Starting Grant (ID: 637860, SLEEPCONTROL), and the University of Marburg. Additional data can be found in the supplement.

Author Contributions

E.M, I.B, F.M., J.B., and M.T. designed, performed, and analyzed experiments. E.M and I.B edited the manuscript. H.B. acquired funding, conceived the project, designed experiments, supervised the work, and wrote the manuscript.

Declarations of Interest

The authors declare that they have no competing interests.

Supplemental Information

Supplemental Information includes 9 figures and 1 table and can be found with this article online.

Materials and Methods

Worm maintenance and strains

C. elegans worms were grown on Nematode Growth Medium (NGM) plates seeded with *E. coli* OP50 and were kept at 15-25°C [74]. Crossed strains were genotyped through Duplex PCR genotyping of single worms [75]. The primer sequences that were used for Duplex PCR can be found below. To confirm the presence of transgenes after crossings, fluorescent markers were used. The following *C. elegans* strains were used:

N2 Wild type (Bristol)

HBR430 *goeIs64[aptf-1p::SL1-GCaMP3.35-SL2::mKate2-unc-54-3'utr, unc-119(+)].*

HBR448 *aptf-1(gk794) II; goeIs64[aptf-1p::SL1-GCaMP3.35-SL2::mKate2-unc-54-3'utr, unc-119(+)].*

HBR531 *yxIs1[glr-1p::GCaMP3, unc-122p::gfp]; aptf-1(gk794) II.*

HBR560 *goeIs120[tdc-1p::SL1-GCaMP3.35-SL2::mKate2-unc-54-3'utr, unc119(+)].*

HBR1118 *aptf-1(gk794)II; goeIs120[tdc-1p::SL1-GCaMP3.35-SL2::mKate2-unc-54-3'utr, unc119(+)].*

HBR1361 *goeIs304[flp-11p::SL1-GCaMP3.35-SL2::mKate2-unc-54-3'UTR, unc-119(+)].*

HBR1374 *goeIs307[flp-11p::ArchT::SL2mKate2-unc-54-3'utr,unc-119(+)]; goeIs304[flp-11p::SL1-GCaMP3.35-SL2::mKate2-unc-54-3'UTR, unc-119(+)].*

HBR1466 *goeIs268[aptf-1p::SL1-GCaMP3.35-SL2::aptf-1-3'utr, unc-119(+)]; goeIs315[flp-11p::ReaChR::mKate2-unc-54-3'UTR, unc-119(+)].*

HBR1472 *goeIs268[aptf-1p::SL1-GCaMP3.35-SL2::aptf-1-3'utr unc-119(+)]; goeIs307[flp-11p::ArchT::SL2mKate-2-unc-54-3'utr, unc-119(+)].*

HBR1478 *goeIs268[aptf-1p::SL1-GCaMP3.35-SL2::aptf-1-3'utr, unc-119(+)]; goeEx557[gcy-13p::ArchT::mKate-2-unc-54-3´-utr, unc-119(+)].*

HBR1482 *goeIs268[aptf-1p::SL1-GCaMP3.35-SL2::aptf-1-3'utr, unc-119(+)];*

	goeEx561[gcy-13p::ReaChR-mKate-2-unc-54-3´-utr, unc-119(+)].
HBR1537	*goeIs268[aptf-1p::SL1-GCaMP3.35-SL2::aptf-1-3'utr, unc-119(+)]; goeIs308[dat-1p::ReaChR::mKate2-unc-54-3'UTR, unc-119(+)].*
HBR1589	*goeIs268[aptf-1p::SL1-GCaMP3.35-SL2::aptf-1-3'utr, unc-119(+)]; goeIs330[nmr-1p::ArchT::mKate-2-unc-54-3'utr, unc-119(+)].*
HBR1597	*goeIs268[aptf-1p::SL1-GCaMP3.35-SL2::aptf-1-3'utr, unc-119(+)], goeIs332[nmr-1p::ReaChR::mKate2-unc-54-3'utr, unc-119(+)].*
HBR1659	*unc-119(ed3) III; goeIs364[tdc-1p::egl-1::SL2-mKate2-unc-54-3'utr, unc-119(+)].*
HBR1753	*wtfIs5[rab-3p::NLS::GCaMP6s; rab-3p::NLS::tagRFP]*
HBR1776	*wtfIs5[rab-3p::NLS::GCaMP6s; rab-3p::NLS::tagRFP]; goeIs307[flp-11 p::ArchT::SL2mKate2-unc-54-3'utr, unc-119(+)]*
HBR1793	*goeIs268[aptf-1p::SL1-GCaMP3.35-SL2::aptf-1-3'utr, unc-119(+)]; goeIs293[tol-1p::ReaChR::mKate2-unc-54-3'utr, unc-119(+)].*
HBR1807	*goeIs232[sra-6p::ReaChR::mKate2-unc-54-3'utr, unc-119(+)]; goeIs304[flp-11p::SL1-GCaMP3.35-SL2::mKate2-unc-54-3'UTR, unc-119(+)].*
HBR1844	*goeIs268[paptf-1p::SL1-GCaMP3.35-SL2::aptf-1-3'utr, unc-119(+)]; goeIs340[dat-1 p::ArchT::SL2mKate2-unc-54-3UTR].*
HBR1845	*goeIs268[paptf-1p::SL1-GCaMP3.35-SL2::aptf-1-3'utr, unc-119(+)];*

655 *goeIs370[lad-2p::ReaChR::mKate2-unc-54-3'UTR, unc-119(+)].*
656
657 HBR1849 *goeIs304[flp-11p::SL1-GCaMP3.35-SL2::mKate2-unc-54-3'UTR,*
658 *unc-119(+)]; goeIs364 [tdc-1p::egl-1::SL2-mkate2-unc-54-3'utr,*
659 *unc-119(+)]; goeIs232[sra-6p::ReaChR::mKate2-unc-54-3'utr,*
660 *unc-119(+)].*
661
662 HBR1873 *goeIs268[paptf-1p::SL1-GCaMP3.35-SL2::aptf-1-3'utr, unc-119(+)];*
663 *goeIs373[lad-2p::ArchT::SL2-mKate2-unc-54-3'UTR, unc-119(+)].*
664
665 HBR1889 *goeIs120[tdc-1p::SL1-GCaMP3.35-SL2::mKate2-unc-54-3'utr,*
666 *unc119(+)]; goeIs232[sra-6p::ReaChR::mKate2-unc-54-3'utr, unc-*
667 *119(+)].*
668
669 HBR1951 *ynIs40[flp-11p::GFP] V; goeIs359 [nmr-1p::egl-1::SL2-mkate2-unc-54-*
670 *3'utr, unc-119(+)].*
671
672 HBR1982 *goeIs402[tol-1p::ArchT::SL2-mKate2-unc-54-3'UTR,unc-119(+)];*
673 *goeIs304[flp-11p::SL1-GCaMP3.35-SL2::mKate2-unc-54-3'UTR, unc-*
674 *119(+)].*
675
676 HBR2019 *akIs11[nmr-1p::ICE]; goeIs307[flp-11p::ArchT::SL2mKate2-unc-54-*
677 *3'utr, unc-119(+)]; goeIs304[flp-11p::SL1-GCaMP3.35-SL2::mKate2-*
678 *unc-54-3'UTR, unc-119(+)].*
679
680 HBR2021 *goeIs307[flp-11p::ArchT::SL2mKate2-unc-54-3'utr,unc-119(+)];*
681 *goeIs304[flp-11p::SL1-GCaMP3.35-SL2::mKate2-unc-54-3'UTR, unc-*
682 *119(+)]; nmr-1(ak4) II.*
683
684 HBR2033 *goeIs195[nmr-1p::SL1-GCaMP6s::mKate2-unc-54-3'utr, unc-119(+)];*
685 *goeIs403[flp-11p::ArchT::mKate2-flp-11-3'utr, unc-119(+)].*

686 HBR2109 *goeIs195[nmr-1p::SL1-GCaMP6s::mKate2-unc-54-3'utr, unc-119(+)];*
687 *goeIs315[flp-11p::ReaChR::mKate2-unc-54-3'UTR, unc-119(+)].*
688
689 HBR2128 *eat-4(ky5) III; goeIs304[flp-11p::SL1-GCaMP3.35-SL2::mKate2-unc-54-*
690 *3'UTR, unc-119(+)].*
691
692 HBR2169 *goeEx718[hlh-34p::ReaChR::mKate2-unc-54-3'UTR,unc-119(+); myo-*
693 *2p::mCherry]; goeIs304[flp-11p::SL1-GCaMP3.35-SL2::mKate2-unc-54-*
694 *3'UTR, unc-119(+)].*
695
696 HBR2180 *goeEx725[hlh-34p::ArchT::SL2mKate2-unc-54-3'UTR, unc-119(+); myo-*
697 *3p::mCherry]; goeIs304[flp-11p::SL1-GCaMP3.35-SL2::mKate2-unc-54-*
698 *3'UTR, unc-119(+)].*
699
700 HBR2231 *goeIs445[ZK673.11p::ArchT::SL2mKate2-unc-54 3' UTR, unc-119(+)].*
701
702 HBR2243 *goeIs445[ZK673.11p::ArchT::SL2mKate2-unc-54 3' UTR, unc-119(+)];*
703 *goeIs5[nmr-1p::SL1-GCaMP3.35-SL2::unc-54-3'utr, unc-119(+)].*
704
705 ZC1148 *yxIs1[glr-1p::GCaMP3.35, unc-122p::gfp].*
706
707 Primers used in this study:
708

	Primer sequence 5'-3'
aptf-1(gk794)	
	CGACAATCTTCCCAAAGACC
	CGGATCGATTGCTAGAGAGG
	GCTTGGACGGCTTTAGTTGA
ArchT	
	ACTTCATCGTCAAGGGATGG
	CATGCAGATGGTGGAGAAGA

ICE	
	CCGAGCTTTGATTGACTCCG
	AGTCATGTCCGAAGCAGTGA
eat-4(ky5)	
	GGGGCGTTTCCTTTTCTTTA
	AAAATGCTCCGACTCCGATT
	ACAGATCCATACGGAAAAGTTC
nmr-1(ak4)	
	TGCTGGTGACTTATGAGCCT
	TGCTGGCGATCTTACTGGAA
	CAACACCGATGCAGAGCTC

709

710

711 **Strain generation**

712

713 DNA constructs were cloned with the three fragments Gateway System (Invitrogen,
714 Carlsbad, CA) into pCG150 to generate new strains [76]. The *ArchT*, the *ReaChR* and the
715 *egl-1* genes were expression-optimized for *C. elegans* [77]. The *tdc-1::egl-1* transgene
716 specifically expresses the apoptosis inducing protein EGL-1 in RIM and RIC. Hence, RIM
717 and RIC are genetically ablated in worms carrying this transgene. The ablation is probably
718 incomplete in L1 worms. The *nmr-1::egl-1* transgene leads to the expression of *egl-1* in all
719 command interneurons causing their genetic ablation. Similar to the *tdc-1::egl-1* transgene,
720 ablation might be incomplete in L1 worms. Transgenic strains were generated by
721 microparticle bombardment or by microinjection. For microparticle bombardment *unc-*
722 *119(ed3)* was used. The rescue of the *unc* phenotype was hence used as a selection marker
723 [78, 79]. The transgenes were backcrossed twice against N2 wild-type worms to remove
724 the *unc-119(ed3)* background. Extrachromosomal arrays were generated by DNA
725 microinjection. DNA was injected in wild-type, mutant or transgenic worms. For injection,
726 DNA was prepared as follows: construct 30-100 ng/µl, co-injection marker 5-50 ng/µl,
727 pCG150 up to a concentration of 100 ng/µl if required. Positive transformants were

selected according to the presence of coinjection markers. The following plasmids were generated for this study:

K31 *nmr-1p::SL1-GCaMP3.35-SL2::mKate2-unc-54-3UTR, unc-119(+)*
K78 *tdc-1p::SL1-GCaMP3.35-SL2::mKate2-unc-54-3UTR, unc-119(+)*
K183 *nmr-1p::ReaChR::mKate2-unc-54-3UTR, unc-119(+)*
K196 *gcy-13p::ArchT::SL2 mKate2 unc-54 3'UTR, unc-119(+)*
K197 *gcy-13p::ReaChR::mKate2-unc-54-3UTR, unc-119(+)*
K200 *nmr-1p::ArchT::SL2 mKate2 unc-54 3'UTR, unc-119(+)*
K204 *tol-1p::ReaChR::mKate2-unc-54-3UTR, unc-119(+)*
K215 *flp11p::ReaChR::SL2mKate2-unc-54-3UTR, unc-119(+)*
K249 *dat-1p::ReaChR::mKate2-unc-54-3UTR, unc-119(+)*
K257 *lad-2p::ReaChR::mKate2-unc-54-3UTR, unc-119(+)*
K259 *dat-1p::ArchT::SL2 mKate2 unc-54 3'UTR, unc-119(+)*
K260 *tol-1p::ArchT::SL2 mKate2 unc-54 3'UTR, unc-119(+)*
K300 *lad-2p::ArchT::SL2 mKate2 unc-54 3'UTR, unc-119(+)*
K308 *tdc-1p::egl-1::SL2mKate2-unc-54-3UTR, unc-119(+)*
K309 *nmr-1p::egl-1::SL2mKate2-unc-54-3UTR, unc-119(+)*
K355 hlh-34p::ReaChR::mKate2-unc-54-3UTR, unc-119(+)
K356 hlh-34p::ArchT::SL2 mKate2 unc-54 3'UTR, unc-119(+)
K364 *ZK673.11p::ArchT::SL2 mKate2 unc-54 3'UTR, unc-119(+)*

Imaging

Cameras and software

All imaging experiments were conducted using either an iXon EMCCD (512x512 pixels), an iXon Ultra EMCCD (1024x1024 pixels), a Photometrics Prime 95B back-illuminated sCMOS camera (1200x1200 pixels) or a Nikon DS Qi2 (4908x3264 pixels). For the iXon cameras the EM Gain was set between 100-200. The exposure times used were between 5-30ms. Andor IQ 2 and 3 and NIS Elements 5 were used for image acquisition.

759

760 Illumination systems

761

762 A standard 100W halogen lamp together with an infrared filter (Semrock Brightline HC
763 785/62) were used for Differential Interference Contrast (DIC) microscopy. For calcium
764 imaging and blue light stimulation an LED illumination (CoolLED) with a 490nm LED
765 and standard GFP filter set (EGFP, Chroma) were used. Optogenetic stimulations and RFP
766 imaging were performed with an LED illumination (CoolLED) with a 585nm LED and
767 standard TexasRed filter set (Chroma).

768

769 **Agarose Microchamber Imaging**

770

771 Long-term imaging experiments were conducted in agarose microchambers as previously
772 described [80, 81]. To summarize, a PDMS mold was used to cast box-shaped indentations
773 in a hydrogel, which consisted of 3% agarose dissolved in S-Basal [82]. Two different sizes
774 were used. We imaged L1 larvae in 190 x 190 x 15 μm microchambers and L4 larvae were
775 imaged in 370 x 370 x 25 μm microchambers. Depending on the developmental state of
776 the worm that was imaged, either pretzel stage eggs or L3 larvae were picked into the
777 chambers with OP50 bacteria. For optogenetic experiments, worms were kept at 25°C
778 before filming. For other experiments, worms were kept at either 20°C or 25°C.

779

780 For time lapse calcium imaging experiments, L1 worms were filmed every 5s (Figure 1A,
781 2D-E, S1E, S2A, S7C), every 8s (Figure S2B-D, S3, S8) or every 10 s (Figure 4) with
782 differential interference contrast (DIC) and widefield fluorescence. The DIC light source
783 was left on continuously and was blocked by a shutter during fluorescence image
784 acquisition. LED illumination was triggered by the EMCCD camera using the TTL
785 exposure output of the camera. An objective with 20x magnification, an LED with 480 nm
786 (light intensity was between 0.15-2 mW/mm^2), and EM gain of 100-200 was used.

787

788 During the continuous experiments in Figure S1E and S2A only DIC images were taken.
789 With the 20x objective and a 0.7 lens 4 worms could be imaged simultaneously in one

790 field. 1-4 fields could be filmed in parallel in one experiment. These image sequences gave
791 measurable neuronal calcium transients and clear DIC images to identify pumping or non-
792 pumping phases.
793
794 **Optogenetic experiments**
795
796 Optogenetic experiments were either conducted in agarose-microchambers as described
797 above or the worms were immobilized. For immobilization experiments the agarose was
798 solved in S-Basal. We used three methods of immobilization for optogenetic experiments.
799 1) Immobilization on a 3% agarose pad with 25mM Levamisole (Sigma Aldrich)
800 (Figure S5).
801 2) Immobilization on a 10% agarose pad with 0.1µm Polybead microspheres
802 (Polyscience) [83] (Figure 1B-C/SDQL, S1A/SDQL, S1D, S2A/SDQL).
803 3) Immobilization on a 10% agarose pad with 0.1µm Polybead microspheres
804 (Polyscience) [83] and 25mM Levamisole (Figure 1B-C/PVC, 2B-C, S1A/PVC,
805 S2A/PVC, S6A).
806
807 Worms were imaged within 30 min of immobilization. A 100x oil objective was used for
808 illumination and imaging. For images in Figure S5A-B a 1.5 lens was added.
809
810 ReaChR for neuronal depolarization or ArchT for hyperpolarization was utilized. For
811 optogenetic stimulation, a 585nm LED and a standard TexasRed (Chroma) filter set were
812 used.
813
814 For optogenetic experiments with L1 larvae, either L4 stage worms or young adult worms
815 were pre-picked onto NGM plates with all-trans-retinal (ATR, Sigma Aldrich) and grown
816 at 25°C. During the two days after exposure to ATR, pretzel stage eggs or L1 worms were
817 taken from this plate for optogenetic experiments. For optogenetic experiments with L4
818 larvae an agar chunk containing a mixed population of growing worms was added to NGM
819 plates containing ATR. Worms for optogenetic experiments were taken from this plate
820 within the next two days.

821

822 Calcium imaging was conducted with an interval of 3s and with an exposure time of 5-
823 30ms. A standard optogenetic protocol included calcium imaging during a baseline. This
824 was followed by a stimulation time, in which the worms were optogenetically stimulated.
825 The 585nm light exposure was continuous except for brief interruptions during the time
826 calcium imaging was conducted. After the optogenetic stimulation, calcium images were
827 acquired during a recovery period.

828

829 In mobile worms this standard protocol was preceded by 20 DIC frames that were taken
830 every 500ms to determine if the worm was pumping. The overall protocol was repeated
831 every 15-30min. L1 mobile worms were imaged with a 20x objective and a 0.7 lens. Mobile
832 L4 worms were imaged with either a 10x objective (Figure 5A-C) or a 20x objective
833 (Figure1B/CEP, 1C/URY, S1A/CEP, S2A/URY). Fixed worms were usually imaged
834 between 1-4 trials. A delay preceded the standard protocol to allow the worm to recover
835 between trials. A 100x oil objective was used for the experiments. To specifically
836 manipulate PVC and SDQL in Figure 1B-C, S1A, S2A, the stimulating illumination was
837 restricted to the neuronal areas. The details for optogenetic experiments can be found in
838 Supplementary Table S1.

839

840 **Blue light stimulation experiments**

841

842 L1 worms were placed in microfluidic-chambers for blue light stimulation experiments.
843 The protocol was repeated every 15min. First, 20 DIC frames were taken every 500ms to
844 determine whether the worm was pumping or not. Next, baseline GCaMP was imaged for
845 3 min, the stimulation phase then lasted 18s and a recovery phase was imaged for 3 min.
846 The 490nm intensity for calcium imaging was 0.07mW/mm^2. The 490nm intensity for
847 stimulation was set to 1.01 mW/mm^2 with a 20x objective. The same LED was used for
848 calcium imaging and stimulation. The intensity levels were controlled with Andor IQ2
849 software.

850

851 The RFP signal of the pan-neuronal strain was imaged in addition to the GCaMP signal
852 during the protocol every 3s with 585nm LED illumination, which was set to
853 0.17mW/mm^2.
854
855 **Spinning Disc Confocal Microscopy**
856
857 L4 worms were fixed with Levamisole. Spinning disc imaging was done with an Andor
858 Revolution disc system using a 488nm (0.34 mW/mm^2) and a 565nm (0.34 mW/mm^2) laser
859 and a Yokogawa (Japan) CSU-X1 spinning disc head. Worms were imaged through a 100x
860 oil objective. In Figure S5A-B an additional 1.5 lens was used. Z-stacks with z-planes
861 0.5µm apart spanning a total distance of 10µm were taken and a maximum intensity
862 projection calculated in ImageJ.
863
864 **Tapping experiment**
865
866 L4 worms were grown and filmed on NGM plates with OP50 bacteria at 20°C. An eyelash
867 was used to gently touch the tail of the worms during L4 lethargus. The time from tail touch
868 until the worms were immobile again was measured with a timer. If worms did not mobilize
869 upon tail touching the time was counted as zero. For GCaMP intensities worms were
870 imaged before and after tail touch each second for a total of 30s. They were illuminated
871 with a Leica EL6000 LED.
872
873 **Image Analysis**
874
875 Image sequences for analysis were selected either based on lethargus or molting timepoints.
876 Lethargus was determined through the DIC images as the non-pumping phase before
877 molting. Time points were classified to be in or outside of lethargus. Typically, the entire
878 lethargus time and two hours before lethargus were analyzed. For some experiments, a
879 certain timespan before molting was analyzed. This timespan was 3h (Figure 2C-D) or 4h
880 (Figure S3D-E). Immobilized worms were classified according to their pumping behavior

881 on NGM plates directly before imaging. Two parameters were extracted from the image
882 sequences.
883
884 1) Calcium transients were extracted in two different ways.
885 A) If only a specific neuron expressed GCaMP, a custom-written MATLAB code
886 automatically detected the position and intensities of the neuron pixels and subtracted the
887 background intensities.
888 B) If more than one neuron expressed GCaMP, a custom-written MATLAB code was used
889 to manually track the intensities and the position of the desired neuron or neuron groups
890 (FigureS8). Background intensities were additionally subtracted from the signal.
891
892 For all stimulation experiments, optogenetic and blue light stimulation experiments, the
893 baseline measurement of each time point was utilized for signal normalization and ΔF/F
894 generation, except for Figure 3A. In Figure 3A, a mean of all baseline intensities for wake
895 time points for each worm was calculated. The mean was then utilized for normalization
896 for all time points for each worm to better show the different RIS activities during wake
897 and sleep. The pan-neuronal signal in Figure S5 was normalized over the measured RFP
898 signal to retrieve ΔR/R. For the transient alignments in Figure 2D, peaks and corresponding
899 speeds were extracted through a custom-written MATLAB script and aligned as time point
900 zero.
901
902 2) The speeds of the worms were calculated from the positions of the tracked neuron,
903 except for the experiments in Figures S2C, S3A. Here, no GCaMP intensity was measured.
904 Frame subtraction of the DIC images was done with a custom-written MATLAB routine
905 instead.
906
907 Baseline extraction
908
909 In Figure 4A, C baseline of RIM GCaMP data was extracted by excluding the 95-100
910 percentile range for wild type and by excluding the 75-100 percentile range for *aptf-*
911 *1(gk794)* mutants. The baseline was smoothed through a second-degree polynomial local

912 regression model and with weighted linear least squares. Zero weight was assigned to data
913 points six means outside the absolute deviation. The amount of data points used for
914 smoothing was three percent.
915
916 **Sleep bout analysis**
917
918 In experiments in Figure 4A, C, S2A, C-D, S8 only the lethargus time was analyzed.
919
920 Sleep bouts were extracted from selected parts of the time-lapse movies. Dependent on the
921 experiment, a specific period of the movie sequence was selected and processed:
922 1) the lethargus period (Figure 4, S2A, C-D, S8)
923 2) the period from two hours before lethargus up to the end of lethargus (Figure 1A,
924 D, S1E, S3A-C, S7)
925 3) either three (Figure 2D-E) or four hours (Figure S3D-E) before molting until
926 molting
927 To extract sleep bouts, speeds and subtraction values were first smoothed. In Figure 1A,
928 D, 2D-E, 5, and S5 speeds were smoothed through a 1st degree polynomial local regression
929 model over 20 time points. Other experiments were smoothed through a second-degree
930 polynomial local regression model and with weighted linear least squares. Zero weight was
931 assigned to data points six means outside the absolute deviation. Data was smoothed either
932 over three percent of all data (Figure S2C-D, S8) or over 40 data points (Figure 4A, C, S3).
933 This was achieved with the *smooth* function in MATLAB. Smoothed speeds were
934 normalized between 0 and 1, with 0 representing the lowest and 1 the highest smoothed
935 speed value of each worm. In order to be scored as a sleep bout, the normalized speed had
936 to be under a defined percentage threshold of the normalized speed for a minimum time.
937 The exact speed and time thresholds were adjusted empirically to represent the worms'
938 behavior [84]. In Figure 2D-E worms had to have a speed below 5% of their maximum
939 smoothed speeds for at least 2min in order to be counted as sleeping. For all other
940 experiments the speed threshold was 10% and the time threshold was 2min. The sleep bout
941 analysis was carried out with a custom-written MATLAB script.
942

943 For stimulation experiments, the baseline and recovery time measurements were too short
944 to include a minimum time threshold in the sleep bout analysis. Hence, immobility was
945 used as a proxy for sleep. A mean of the wake speeds was calculated for each worm. In
946 most experiments a worm was counted as sleeping when its speed was below 10% of the
947 calculated mean of the wake speeds. In Figure 3A, C the threshold was adjusted to 30%
948 and in Figure S6 to 50% to account for a different locomotor behavior of the worms. RIS
949 signals and speeds of wild type and mutants were aligned to sleep bout onset for
950 comparison in Figure S2C, S3C, D. For GCaMP normalization ten data points before sleep
951 bout onset were taken as baseline in order to calculate ΔF/F. In Figure S7C motion bouts
952 were assigned whenever there was no detected sleep bout.
953
954 **Fitting**
955
956 The data in Figure 3B was fitted to an asymptote with Origin software. The data in Figure
957 S5 was fitted to a logistic regression using Origin software. Exact functions and R^2 values
958 can be found in the respective figures.
959
960 **Statistics**

961 Sample sizes were determined empirically based on previous studies. If possible,
962 experiments were carried out with internal controls. If this was not possible, control and
963 experimental condition were alternated. Researchers were not blinded to the genotype for
964 data analysis, as data analysis was performed by automated routines. Sample exclusion is
965 described in the respective methods section. To compare GCaMP intensities and speeds of
966 one sample group at different time points the Wilcoxon signed-rank test was utilized. The
967 Fisher's Exact Test was used to compare the sleep fractions of one sample group at
968 different time points. The entirety of the baseline was compared to the entirety of the
969 stimulation period unless otherwise stated through significance bars. Data from different
970 strains was either compared with the Kolmogorov-Smirnov-Test or the Welch test. The p-
971 values can be taken from the respective Figure descriptions. In the graph depicted is the
972 mean +/- SEM unless otherwise stated. The box in the box plots represents the inter quartile

range with the median. The whiskers show the 10-90-percentile range. The individual data points are furthermore plotted on top of the box.

976 **References**

977

978 1. Irwin MR. Why sleep is important for health: a psychoneuroimmunology
979 perspective. Annu Rev Psychol. 2015;66:143-72. Epub 2014/07/26. doi:
980 10.1146/annurev-psych-010213-115205. PubMed PMID: 25061767; PubMed Central
981 PMCID: PMCPMC4961463.
982 2. Drake CL, Roehrs T, Roth T. Insomnia causes, consequences, and therapeutics:
983 an overview. Depression and anxiety. 2003;18(4):163-76. Epub 2003/12/09. doi:
984 10.1002/da.10151. PubMed PMID: 14661186.
985 3. Van Cauter E, Spiegel K, Tasali E, Leproult R. Metabolic consequences of sleep
986 and sleep loss. Sleep Med. 2008;9 Suppl 1:S23-8. Epub 2008/12/17. doi: 10.1016/S1389-
987 9457(08)70013-3. PubMed PMID: 18929315; PubMed Central PMCID:
988 PMCPMC4444051.
989 4. Knutson KL, Spiegel K, Penev P, Van Cauter E. The metabolic consequences of
990 sleep deprivation. Sleep medicine reviews. 2007;11(3):163-78. Epub 2007/04/20. doi:
991 10.1016/j.smrv.2007.01.002. PubMed PMID: 17442599; PubMed Central PMCID:
992 PMCPMC1991337.
993 5. Marder E. Neuromodulation of neuronal circuits: back to the future. Neuron.
994 2012;76(1):1-11. Epub 2012/10/09. doi: 10.1016/j.neuron.2012.09.010. PubMed PMID:
995 23040802; PubMed Central PMCID: PMC3482119.
996 6. Mayford M, Siegelbaum SA, Kandel ER. Synapses and memory storage. Cold
997 Spring Harbor perspectives in biology. 2012;4(6). Epub 2012/04/13. doi:
998 10.1101/cshperspect.a005751. PubMed PMID: 22496389; PubMed Central PMCID:
999 PMC3367555.
1000 7. Hafting T, Fyhn M, Molden S, Moser MB, Moser EI. Microstructure of a spatial
1001 map in the entorhinal cortex. Nature. 2005;436(7052):801-6. Epub 2005/06/21. doi:
1002 10.1038/nature03721. PubMed PMID: 15965463.
1003 8. Saper CB, Fuller PM, Pedersen NP, Lu J, Scammell TE. Sleep state switching.
1004 Neuron. 2010;68(6):1023-42. Epub 2010/12/22. doi: 10.1016/j.neuron.2010.11.032.
1005 PubMed PMID: 21172606; PubMed Central PMCID: PMC3026325.
1006 9. Campbell SS, Tobler I. Animal sleep: a review of sleep duration across
1007 phylogeny. Neurosci Biobehav Rev. 1984;8(3):269-300. Epub 1984/01/01. PubMed
1008 PMID: 6504414.
1009 10. Bringmann H. Sleep-Active Neurons: Conserved Motors of Sleep. Genetics.
1010 2018;208(4):1279-89. Epub 2018/04/06. doi: 10.1534/genetics.117.300521. PubMed
1011 PMID: 29618588; PubMed Central PMCID: PMC5887131.
1012 11. Lu J, Sherman D, Devor M, Saper CB. A putative flip-flop switch for control of
1013 REM sleep. Nature. 2006;441(7093):589-94. Epub 2006/05/12. doi:
1014 10.1038/nature04767. PubMed PMID: 16688184.
1015 12. Morairty S, Rainnie D, McCarley R, Greene R. Disinhibition of ventrolateral
1016 preoptic area sleep-active neurons by adenosine: a new mechanism for sleep promotion.
1017 Neuroscience. 2004;123(2):451-7. Epub 2003/12/31. PubMed PMID: 14698752.
1018 13. Saper CB, Scammell TE, Lu J. Hypothalamic regulation of sleep and circadian
1019 rhythms. Nature. 2005;437(7063):1257-63. Epub 2005/10/28. doi: 10.1038/nature04284.
1020 PubMed PMID: 16251950.

1021 14. Weber F, Dan Y. Circuit-based interrogation of sleep control. Nature.
1022 2016;538(7623):51-9. Epub 2016/10/07. doi: 10.1038/nature19773. PubMed PMID:
1023 27708309.
1024 15. Zhang Z, Zhong P, Hu F, Barger Z, Ren Y, Ding X, et al. An Excitatory Circuit in
1025 the Perioculomotor Midbrain for Non-REM Sleep Control. Cell. 2019;177(5):1293-307
1026 e16. Epub 2019/04/30. doi: 10.1016/j.cell.2019.03.041. PubMed PMID: 31031008.
1027 16. Borbely AA. A two process model of sleep regulation. Human neurobiology.
1028 1982;1(3):195-204. Epub 1982/01/01. PubMed PMID: 7185792.
1029 17. Frank MG. Astroglial regulation of sleep homeostasis. Curr Opin Neurobiol.
1030 2013;23(5):812-8. Epub 2013/03/23. doi: 10.1016/j.conb.2013.02.009. PubMed PMID:
1031 23518138.
1032 18. Krueger JM, Frank MG, Wisor JP, Roy S. Sleep function: Toward elucidating an
1033 enigma. Sleep medicine reviews. 2016;28:46-54. Epub 2015/10/09. doi:
1034 10.1016/j.smrv.2015.08.005. PubMed PMID: 26447948; PubMed Central PMCID:
1035 PMC4769986.
1036 19. Donlea JM, Pimentel D, Miesenbock G. Neuronal machinery of sleep
1037 homeostasis in Drosophila. Neuron. 2014;81(4):860-72. Epub 2014/02/25. doi:
1038 10.1016/j.neuron.2013.12.013. PubMed PMID: 24559676; PubMed Central PMCID:
1039 PMC3969244.
1040 20. Pimentel D, Donlea JM, Talbot CB, Song SM, Thurston AJ, Miesenbock G.
1041 Operation of a homeostatic sleep switch. Nature. 2016;536(7616):333-7. Epub
1042 2016/08/04. doi: 10.1038/nature19055. PubMed PMID: 27487216; PubMed Central
1043 PMCID: PMC4998959.
1044 21. Halasz P. Hierarchy of micro-arousals and the microstructure of sleep.
1045 Neurophysiologie clinique = Clinical neurophysiology. 1998;28(6):461-75. Epub
1046 1999/01/23. PubMed PMID: 9894227.
1047 22. Amzica F, Steriade M. Cellular substrates and laminar profile of sleep K-
1048 complex. Neuroscience. 1998;82(3):671-86. Epub 1998/03/04. PubMed PMID: 9483527.
1049 23. Cash SS, Halgren E, Dehghani N, Rossetti AO, Thesen T, Wang C, et al. The
1050 human K-complex represents an isolated cortical down-state. Science.
1051 2009;324(5930):1084-7. Epub 2009/05/23. doi: 10.1126/science.1169626. PubMed
1052 PMID: 19461004; PubMed Central PMCID: PMC3715654.
1053 24. Iwanir S, Tramm N, Nagy S, Wright C, Ish D, Biron D. The microarchitecture of
1054 C. elegans behavior during lethargus: homeostatic bout dynamics, a typical body posture,
1055 and regulation by a central neuron. sleep. 2013;36(3):385-95. Epub 2013/03/02. doi:
1056 10.5665/sleep.2456. PubMed PMID: 23449971; PubMed Central PMCID: PMC3571756.
1057 25. Nagy S, Tramm N, Sanders J, Iwanir S, Shirley IA, Levine E, et al. Homeostasis
1058 in C. elegans sleep is characterized by two behaviorally and genetically distinct
1059 mechanisms. eLife. 2014;3:e04380. Epub 2014/12/05. doi: 10.7554/eLife.04380.
1060 PubMed PMID: 25474127; PubMed Central PMCID: PMC4273442.
1061 26. Joiner WJ. Unraveling the Evolutionary Determinants of Sleep. Curr Biol.
1062 2016;26(20):R1073-R87. Epub 2016/10/26. doi: 10.1016/j.cub.2016.08.068. PubMed
1063 PMID: 27780049; PubMed Central PMCID: PMC5120870.
1064 27. Turek M, Lewandrowski I, Bringmann H. An AP2 transcription factor is required
1065 for a sleep-active neuron to induce sleep-like quiescence in C. elegans. Curr Biol.

1066 2013;23(22):2215-23. Epub 2013/11/05. doi: 10.1016/j.cub.2013.09.028. PubMed PMID:
1067 24184105.
1068 28. Bennett HL, Khoruzhik Y, Hayden D, Huang H, Sanders J, Walsh MB, et al.
1069 Normal sleep bouts are not essential for C. elegans survival and FoxO is important for
1070 compensatory changes in sleep. BMC neuroscience. 2018;19(1):10. Epub 2018/03/11.
1071 doi: 10.1186/s12868-018-0408-1. PubMed PMID: 29523076.
1072 29. Wu Y, Masurat F, Preis J, Bringmann H. Sleep Counteracts Aging Phenotypes to
1073 Survive Starvation-Induced Developmental Arrest in C. elegans. Curr Biol.
1074 2018;28(22):3610-24 e8. Epub 2018/11/13. doi: 10.1016/j.cub.2018.10.009. PubMed
1075 PMID: 30416057; PubMed Central PMCID: PMCPMC6264389.
1076 30. White JG, Southgate E, Thomson JN, Brenner S. The structure of the nervous
1077 system of the nematode Caenorhabditis elegans. Philos Trans R Soc Lond B Biol Sci.
1078 1986;314(1165):1-340. Epub 1986/11/12. PubMed PMID: 22462104.
1079 31. Raizen DM, Zimmerman JE, Maycock MH, Ta UD, You YJ, Sundaram MV, et
1080 al. Lethargus is a Caenorhabditis elegans sleep-like state. Nature. 2008;451(7178):569-
1081 72. Epub 2008/01/11. doi: nature06535 [pii]10.1038/nature06535. PubMed PMID:
1082 18185515.
1083 32. Trojanowski NF, Raizen DM. Call it Worm Sleep. Trends in neurosciences.
1084 2016;39(2):54-62. Epub 2016/01/10. doi: 10.1016/j.tins.2015.12.005. PubMed PMID:
1085 26747654; PubMed Central PMCID: PMC4738085.
1086 33. Kayser MS, Biron D. Sleep and Development in Genetically Tractable Model
1087 Organisms. Genetics. 2016;203(1):21-33. Epub 2016/05/18. doi:
1088 10.1534/genetics.116.189589. PubMed PMID: 27183564; PubMed Central PMCID:
1089 PMC4858775.
1090 34. Sulston JE, Horvitz HR. Post-embryonic cell lineages of the nematode,
1091 Caenorhabditis elegans. Dev Biol. 1977;56(1):110-56. Epub 1977/03/01. doi: 0012-
1092 1606(77)90158-0 [pii]. PubMed PMID: 838129.
1093 35. Cassada RC, Russell RL. The dauerlarva, a post-embryonic developmental variant
1094 of the nematode Caenorhabditis elegans. Dev Biol. 1975;46(2):326-42. Epub 1975/10/01.
1095 doi: 0012-1606(75)90109-8 [pii]. PubMed PMID: 1183723.
1096 36. Han X, Chow BY, Zhou H, Klapoetke NC, Chuong A, Rajimehr R, et al. A high-
1097 light sensitivity optical neural silencer: development and application to optogenetic
1098 control of non-human primate cortex. Frontiers in systems neuroscience. 2011;5:18. Epub
1099 2011/08/04. doi: 10.3389/fnsys.2011.00018. PubMed PMID: 21811444; PubMed Central
1100 PMCID: PMC3082132.
1101 37. Okazaki A, Takagi S. An optogenetic application of proton pump ArchT to C.
1102 elegans cells. Neuroscience research. 2013;75(1):29-34. Epub 2012/10/10. doi:
1103 10.1016/j.neures.2012.09.002. PubMed PMID: 23044183.
1104 38. Alkema MJ, Hunter-Ensor M, Ringstad N, Horvitz HR. Tyramine Functions
1105 independently of octopamine in the Caenorhabditis elegans nervous system. Neuron.
1106 2005;46(2):247-60. Epub 2005/04/26. doi: S0896-6273(05)00167-4 [pii]
1107 10.1016/j.neuron.2005.02.024. PubMed PMID: 15848803.
1108 39. Gordus A, Pokala N, Levy S, Flavell SW, Bargmann CI. Feedback from network
1109 states generates variability in a probabilistic olfactory circuit. Cell. 2015;161(2):215-27.
1110 Epub 2015/03/17. doi: 10.1016/j.cell.2015.02.018. PubMed PMID: 25772698; PubMed
1111 Central PMCID: PMC4821011.

1112 40. Kawano T, Po MD, Gao S, Leung G, Ryu WS, Zhen M. An imbalancing act: gap
1113 junctions reduce the backward motor circuit activity to bias C. elegans for forward
1114 locomotion. Neuron. 2011;72(4):572-86. Epub 2011/11/22. doi:
1115 10.1016/j.neuron.2011.09.005. PubMed PMID: 22099460.
1116 41. Zimmer M, Gray JM, Pokala N, Chang AJ, Karow DS, Marletta MA, et al.
1117 Neurons detect increases and decreases in oxygen levels using distinct guanylate
1118 cyclases. Neuron. 2009;61(6):865-79. Epub 2009/03/28. doi:
1119 10.1016/j.neuron.2009.02.013. PubMed PMID: 19323996; PubMed Central PMCID:
1120 PMCPMC2760494.
1121 42. Sawin ER, Ranganathan R, Horvitz HR. C. elegans locomotory rate is modulated
1122 by the environment through a dopaminergic pathway and by experience through a
1123 serotonergic pathway. Neuron. 2000;26(3):619-31. Epub 2000/07/15. doi: S0896-
1124 6273(00)81199-X [pii]. PubMed PMID: 10896158.
1125 43. Zheng Y, Brockie PJ, Mellem JE, Madsen DM, Maricq AV. Neuronal control of
1126 locomotion in C. elegans is modified by a dominant mutation in the GLR-1 ionotropic
1127 glutamate receptor. Neuron. 1999;24(2):347-61. Epub 1999/11/26. PubMed PMID:
1128 10571229.
1129 44. Cao J, Packer JS, Ramani V, Cusanovich DA, Huynh C, Daza R, et al.
1130 Comprehensive single-cell transcriptional profiling of a multicellular organism. Science.
1131 2017;357(6352):661-7. Epub 2017/08/19. doi: 10.1126/science.aam8940. PubMed
1132 PMID: 28818938; PubMed Central PMCID: PMC5894354.
1133 45. Packer JSZ, Q., Huynh CS, P., Preston E, Dueck HS, D., Tan K, Trapnell C, et al.
1134 A lineage-resolved molecular atlas of C. elegans embryogenesis at single cell resolution.
1135 BioArxive. 2019;(8). doi: 10.1101/565549
1136 46. Chalfie M, Sulston JE, White JG, Southgate E, Thomson JN, Brenner S. The
1137 neural circuit for touch sensitivity in Caenorhabditis elegans. J Neurosci. 1985;5(4):956-
1138 64. Epub 1985/04/01. PubMed PMID: 3981252.
1139 47. Li W, Kang L, Piggott BJ, Feng Z, Xu XZ. The neural circuits and sensory
1140 channels mediating harsh touch sensation in Caenorhabditis elegans. Nat Commun.
1141 2011;2:315. Epub 2011/05/19. doi: 10.1038/ncomms1308. PubMed PMID: 21587232;
1142 PubMed Central PMCID: PMC3098610.
1143 48. Turek M, Besseling J, Spies JP, Konig S, Bringmann H. Sleep-active neuron
1144 specification and sleep induction require FLP-11 neuropeptides to systemically induce
1145 sleep. eLife. 2016;5. Epub 2016/03/08. doi: 10.7554/eLife.12499. PubMed PMID:
1146 26949257; PubMed Central PMCID: PMC4805538.
1147 49. Brockie PJ, Mellem JE, Hills T, Madsen DM, Maricq AV. The C. elegans
1148 glutamate receptor subunit NMR-1 is required for slow NMDA-activated currents that
1149 regulate reversal frequency during locomotion. Neuron. 2001;31(4):617-30. Epub
1150 2001/09/08. PubMed PMID: 11545720.
1151 50. Singh K, Ju JY, Walsh MB, DiIorio MA, Hart AC. Deep Conservation of Genes
1152 Required for Both Drosphila melanogaster and Caenorhabditis elegans Sleep Includes a
1153 Role for Dopaminergic Signaling. sleep. 2014;37(9). PubMed PMID: 25142568.
1154 51. Schwarz J, Bringmann H. Reduced sleep-like quiescence in both hyperactive and
1155 hypoactive mutants of the Galphaq Gene egl-30 during lethargus in Caenorhabditis
1156 elegans. PLoS One. 2013;8(9):e75853. Epub 2013/09/28. doi:

1157 10.1371/journal.pone.0075853. PubMed PMID: 24073282; PubMed Central PMCID:
1158 PMC3779211.
1159 52. Huang H, Hayden DJ, Zhu CT, Bennett HL, Venkatachalam V, Skuja LL, et al.
1160 Gap Junctions and NCA Cation Channels Are Critical for Developmentally Timed Sleep
1161 and Arousal in Caenorhabditis elegans. Genetics. 2018;210(4):1369-81. Epub
1162 2018/10/17. doi: 10.1534/genetics.118.301551. PubMed PMID: 30323068; PubMed
1163 Central PMCID: PMCPMC6283151.
1164 53. Pirri JK, Alkema MJ. The neuroethology of C. elegans escape. Curr Opin
1165 Neurobiol. 2012;22(2):187-93. Epub 2012/01/10. doi: 10.1016/j.conb.2011.12.007.
1166 PubMed PMID: 22226513; PubMed Central PMCID: PMCPMC3437330.
1167 54. Nichols ALA, Eichler T, Latham R, Zimmer M. A global brain state underlies C.
1168 elegans sleep behavior. Science. 2017;356(6344). Epub 2017/06/24. doi:
1169 10.1126/science.aam6851. PubMed PMID: 28642382.
1170 55. Kaplan JM, Horvitz HR. A dual mechanosensory and chemosensory neuron in
1171 Caenorhabditis elegans. Proc Natl Acad Sci U S A. 1993;90(6):2227-31. Epub
1172 1993/03/15. PubMed PMID: 8460126.
1173 56. Guo ZV, Hart AC, Ramanathan S. Optical interrogation of neural circuits in
1174 Caenorhabditis elegans. Nat Methods. 2009;6(12):891-6. Epub 2009/11/10. doi:
1175 nmeth.1397 [pii]
1176 10.1038/nmeth.1397. PubMed PMID: 19898486.
1177 57. Husson SJ, Costa WS, Wabnig S, Stirman JN, Watson JD, Spencer WC, et al.
1178 Optogenetic analysis of a nociceptor neuron and network reveals ion channels acting
1179 downstream of primary sensors. Curr Biol. 2012;22(9):743-52. Epub 2012/04/10. doi:
1180 10.1016/j.cub.2012.02.066. PubMed PMID: 22483941; PubMed Central PMCID:
1181 PMC3350619.
1182 58. Stirman JN, Crane MM, Husson SJ, Wabnig S, Schultheis C, Gottschalk A, et al.
1183 Real-time multimodal optical control of neurons and muscles in freely behaving
1184 Caenorhabditis elegans. Nat Methods. 2011;8(2):153-8. Epub 2011/01/18. doi:
1185 10.1038/nmeth.1555. PubMed PMID: 21240278; PubMed Central PMCID:
1186 PMC3189501.
1187 59. Kato S, Kaplan HS, Schrodel T, Skora S, Lindsay TH, Yemini E, et al. Global
1188 brain dynamics embed the motor command sequence of Caenorhabditis elegans. Cell.
1189 2015;163(3):656-69. Epub 2015/10/20. doi: 10.1016/j.cell.2015.09.034. PubMed PMID:
1190 26478179.
1191 60. Schwarz J, Lewandrowski I, Bringmann H. Reduced activity of a sensory neuron
1192 during a sleep-like state in Caenorhabditis elegans. Curr Biol. 2011;21(24):R983-4. Epub
1193 2011/12/24. doi: S0960-9822(11)01207-3[pii]10.1016/j.cub.2011.10.046. PubMed
1194 PMID: 22192827.
1195 61. Cho JY, Sternberg PW. Multilevel modulation of a sensory motor circuit during
1196 C. elegans sleep and arousal. Cell. 2014;156(1-2):249-60. Epub 2014/01/21. doi:
1197 10.1016/j.cell.2013.11.036. PubMed PMID: 24439380; PubMed Central PMCID:
1198 PMC3962823.
1199 62. Skora S, Mende F, Zimmer M. Energy Scarcity Promotes a Brain-wide Sleep
1200 State Modulated by Insulin Signaling in C. elegans. Cell reports. 2018;22(4):953-66.
1201 Epub 2018/02/02. doi: 10.1016/j.celrep.2017.12.091. PubMed PMID: 29386137.

1202 63. Katz M, Corson F, Iwanir S, Biron D, Shaham S. Glia Modulate a Neuronal
1203 Circuit for Locomotion Suppression during Sleep in C. elegans. Cell reports.
1204 2018;22(10):2575-83. Epub 2018/03/08. doi: 10.1016/j.celrep.2018.02.036. PubMed
1205 PMID: 29514087; PubMed Central PMCID: PMCPMC5870883.
1206 64. Schrodel T, Prevedel R, Aumayr K, Zimmer M, Vaziri A. Brain-wide 3D imaging
1207 of neuronal activity in Caenorhabditis elegans with sculpted light. Nat Methods.
1208 2013;10(10):1013-20. Epub 2013/09/10. doi: 10.1038/nmeth.2637. PubMed PMID:
1209 24013820.
1210 65. Gallagher T, Kim J, Oldenbroek M, Kerr R, You YJ. ASI regulates satiety
1211 quiescence in C. elegans. J Neurosci. 2013;33(23):9716-24. Epub 2013/06/07. doi:
1212 10.1523/JNEUROSCI.4493-12.2013. PubMed PMID: 23739968; PubMed Central
1213 PMCID: PMCPMC3726252.
1214 66. Goetting DL, Soto R, Van Buskirk C. Food-Dependent Plasticity in
1215 Caenorhabditis elegans Stress-Induced Sleep Is Mediated by TOR-FOXA and TGF-beta
1216 Signaling. Genetics. 2018. Epub 2018/06/22. doi: 10.1534/genetics.118.301204. PubMed
1217 PMID: 29925566.
1218 67. Spies J, Bringmann H. Automated detection and manipulation of sleep in C.
1219 elegans reveals depolarization of a sleep-active neuron during mechanical stimulation-
1220 induced sleep deprivation. Sci Rep. 2018;8(1):9732. Epub 2018/06/29. doi:
1221 10.1038/s41598-018-28095-5. PubMed PMID: 29950594.
1222 68. Scholz M, Linder AN, Randi F, Sharma AK, Yu X, Shaevitz JW, et al. Predicting
1223 natural behavior from whole-brain neural dynamics. Biorxive. 2018:445643v1. Epub
1224 October 17, 2018. doi: https://doi.org/10.1101/445643
1225 69. Chrousos G, Vgontzas AN, Kritikou I. HPA Axis and Sleep. In: De Groot LJ,
1226 Chrousos G, Dungan K, Feingold KR, Grossman A, Hershman JM, et al., editors.
1227 Endotext. South Dartmouth (MA): Endotext.org; 2016.
1228 70. Panossian LA, Avidan AY. Review of sleep disorders. The Medical clinics of
1229 North America. 2009;93(2):407-25, ix. Epub 2009/03/11. doi:
1230 10.1016/j.mcna.2008.09.001. PubMed PMID: 19272516.
1231 71. Liu S, Liu Q, Tabuchi M, Wu MN. Sleep Drive Is Encoded by Neural Plastic
1232 Changes in a Dedicated Circuit. Cell. 2016;165(6):1347-60. Epub 2016/05/24. doi:
1233 10.1016/j.cell.2016.04.013. PubMed PMID: 27212237; PubMed Central PMCID:
1234 PMC4892967.
1235 72. Donlea JM, Pimentel D, Talbot CB, Kempf A, Omoto JJ, Hartenstein V, et al.
1236 Recurrent Circuitry for Balancing Sleep Need and Sleep. Neuron. 2018;97(2):378-89 e4.
1237 Epub 2018/01/09. doi: 10.1016/j.neuron.2017.12.016. PubMed PMID: 29307711;
1238 PubMed Central PMCID: PMCPMC5779612.
1239 73. Dijk DJ. Regulation and functional correlates of slow wave sleep. Journal of
1240 clinical sleep medicine : JCSM : official publication of the American Academy of Sleep
1241 Medicine. 2009;5(2 Suppl):S6-15. Epub 2009/12/17. PubMed PMID: 19998869; PubMed
1242 Central PMCID: PMC2824213.
1243 74. Brenner S. The genetics of Caenorhabditis elegans. Genetics. 1974;77(1):71-94.
1244 Epub 1974/05/01. PubMed PMID: 4366476.
1245 75. Ahringer A. Reverse genetics. WormBook, ed The C elegans Research
1246 Community. 2006. doi: doi/10.1895/wormbook.1.47.1.

1247 76. Merritt C, Seydoux G. Transgenic solutions for the germline. WormBook.
1248 2010:1-21. Epub 2010/02/20. doi: 10.1895/wormbook.1.148.1. PubMed PMID:
1249 20169625.
1250 77. Redemann S, Schloissnig S, Ernst S, Pozniakowsky A, Ayloo S, Hyman AA, et
1251 al. Codon adaptation-based control of protein expression in C. elegans. Nat Methods.
1252 2011;8(3):250-2. Epub 2011/02/01. doi: nmeth.1565 [pii]10.1038/nmeth.1565. PubMed
1253 PMID: 21278743.
1254 78. Praitis V, Casey E, Collar D, Austin J. Creation of low-copy integrated transgenic
1255 lines in Caenorhabditis elegans. Genetics. 2001;157(3):1217-26. Epub 2001/03/10.
1256 PubMed PMID: 11238406; PubMed Central PMCID: PMC1461581.
1257 79. Wilm T, Demel P, Koop HU, Schnabel H, Schnabel R. Ballistic transformation of
1258 Caenorhabditis elegans. Gene. 1999;229(1-2):31-5. Epub 1999/03/30. PubMed PMID:
1259 10095101.
1260 80. Bringmann H. Agarose hydrogel microcompartments for imaging sleep- and
1261 wake-like behavior and nervous system development in Caenorhabditis elegans larvae. J
1262 Neurosci Methods. 2011;201(1):78-88. Epub 2011/08/02. doi: S0165-0270(11)00418-3
1263 [pii]10.1016/j.jneumeth.2011.07.013. PubMed PMID: 21801751.
1264 81. Turek M, Besseling J, Bringmann H. Agarose Microchambers for Long-term
1265 Calcium Imaging of Caenorhabditis elegans. Journal of visualized experiments : JoVE.
1266 2015;(100):e52742. Epub 2015/07/02. doi: 10.3791/52742. PubMed PMID: 26132740;
1267 PubMed Central PMCID: PMC4544933.
1268 82. Stiernagle T. Maintenance of C. elegans. WormBook. 2006:1-11. Epub
1269 2007/12/01. doi: 10.1895/wormbook.1.101.1. PubMed PMID: 18050451.
1270 83. Kim E, Sun L, Gabel CV, Fang-Yen C. Long-term imaging of Caenorhabditis
1271 elegans using nanoparticle-mediated immobilization. PLoS One. 2013;8(1):e53419. Epub
1272 2013/01/10. doi: 10.1371/journal.pone.0053419. PubMed PMID: 23301069; PubMed
1273 Central PMCID: PMCPMC3536676.
1274 84. Nagy S, Raizen DM, Biron D. Measurements of behavioral quiescence in
1275 Caenorhabditis elegans. Methods. 2014. Epub 2014/03/20. doi:
1276 10.1016/j.ymeth.2014.03.009. PubMed PMID: 24642199.
1277

1278 **Figures**

1279

1280 **Figure 1**

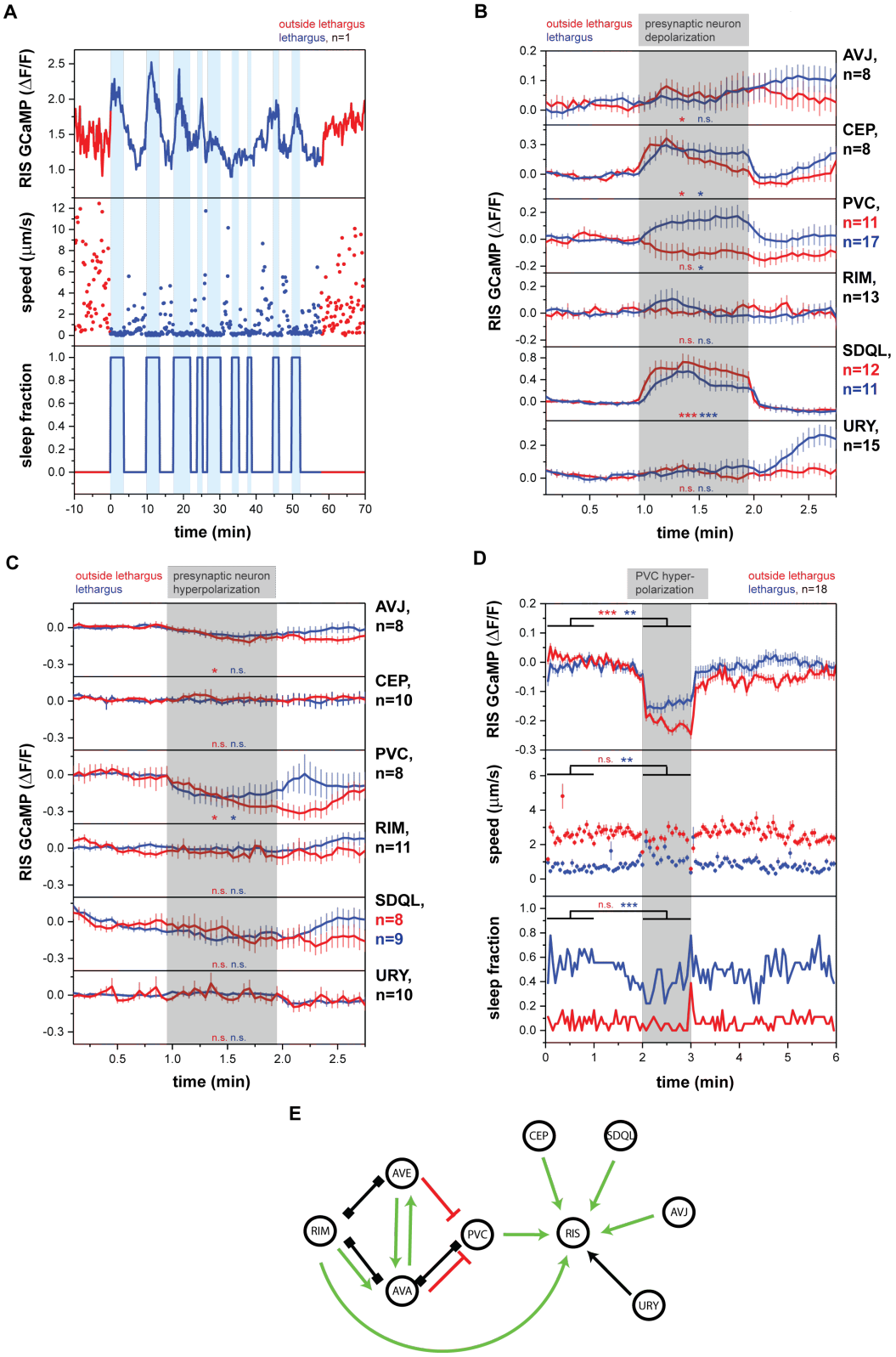

1281

1282 **Figure 1**

1283 **Presynaptic neurons control the activity of the sleep-active RIS neuron**

1284 A) Sample trace of RIS activity and worm locomotion behavior outside of and in
1285 lethargus. RIS is relatively inactive outside of lethargus and shows strong activity
1286 transients in lethargus. Upon RIS activation, worms enter sleep bouts.

1287 B) Presynaptic neurons activate RIS outside of and in lethargus. For statistical
1288 calculations neural activities before the stimulation period (0 - 0.95 min) were
1289 compared to activity levels during the stimulation period (1 - 1.95 min); *$p <$
1290 0.05, **$p < 0.01$, ***$p < 0.001$, Wilcoxon Signed Rank Test.

1291 C) PVC is essential for lethargus-specific RIS activation; Statistical calculations
1292 were performed as described in B, but in experiments, in which SDQL was
1293 stimulated baseline activity levels were calculated over the time interval from 0.6
1294 - 0.95 min; *$p < 0.05$, Wilcoxon Signed Rank Test.

1295 D) PVC hyperpolarization inactivates RIS and induces behavioral activity; **$p <$
1296 0.01, ***$p < 0.001$, Wilcoxon Signed Rank Test for GCaMP and speed, Fisher's
1297 Exact Test for sleep fraction.

1298 E) Circuit model of the RIS presynaptic regulatory network. Presynaptic neurons
1299 present mostly activators of RIS. PVC is essential for lethargus-specific RIS
1300 activation. Effects of presynaptic neurons might be mostly direct, except for RIM.

1301

1302 **Figure 2**

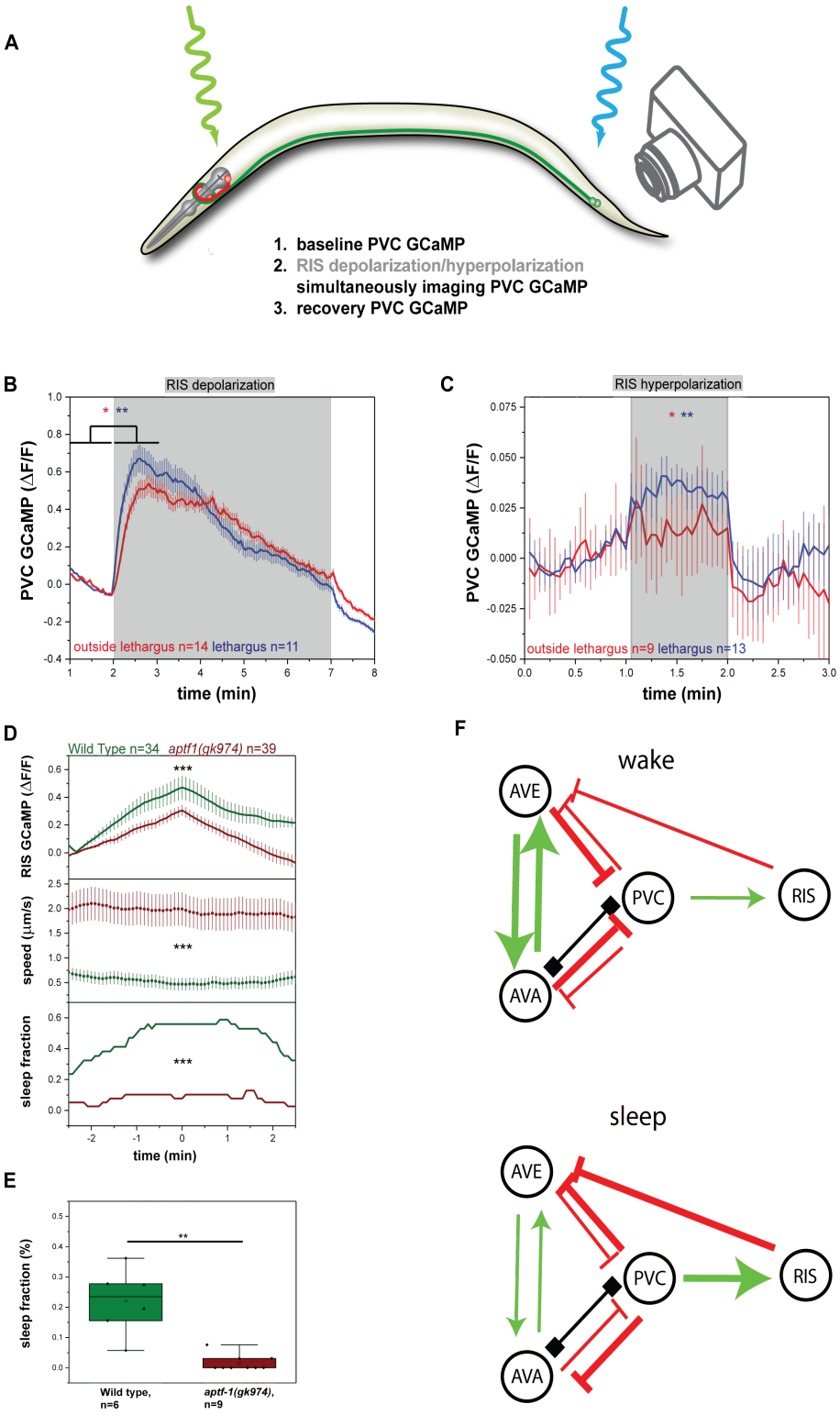

1303

1304 **Figure 2**

1305 **RIS and PVC activate each other forming a positive feedback loop**

1306 A) The experimental set up. First, a baseline of PVC was measured through calcium
1307 imaging. Then, RIS was optogenetically manipulated while PVC was
1308 simultaneously calcium imaged. Finally, a recovery period was imaged of PVC.

1309 B) RIS depolarization leads to a strong PVC depolarization outside and during
1310 lethargus; *$p < 0.05$, **$p < 0.01$, Wilcoxon Signed Rank Test.

1311 C) RIS hyperpolarization leads to a weak PVC depolarization outside and in
1312 lethargus. For statistical calculations neural activities before the stimulation
1313 period (0 - 1 min) were compared to activity levels during the stimulation period
1314 (1 - 2 min); *$p < 0.05$, **$p < 0.01$, compared before and during stimulation,
1315 Wilcoxon Signed Rank Test.

1316 D) RIS does not reach the same activation levels in *aptf-1(gk794)* mutants compared
1317 to wild-type worms. *aptf-1(gk794)* mutants do neither immobilize nor sleep
1318 during RIS activation; ***$p < 0.001$, Welch Test.

1319 E) *aptf-1(gk794)* mutants do not show sleep during lethargus; **$p < 0.01$,
1320 Kolmogorov-Smirnov-Test.

1321 F) A circuit model for the positive feedback loop between RIS and PVC. During
1322 wakefulness, reverse command interneurons inhibit PVC so that PVC does not
1323 activate RIS. In lethargus, PVC is directly activating RIS, which then inhibits
1324 reverse command interneurons. This may speculatively disinhibit PVC, leading to
1325 a positive feedback.

1326

Figure 3

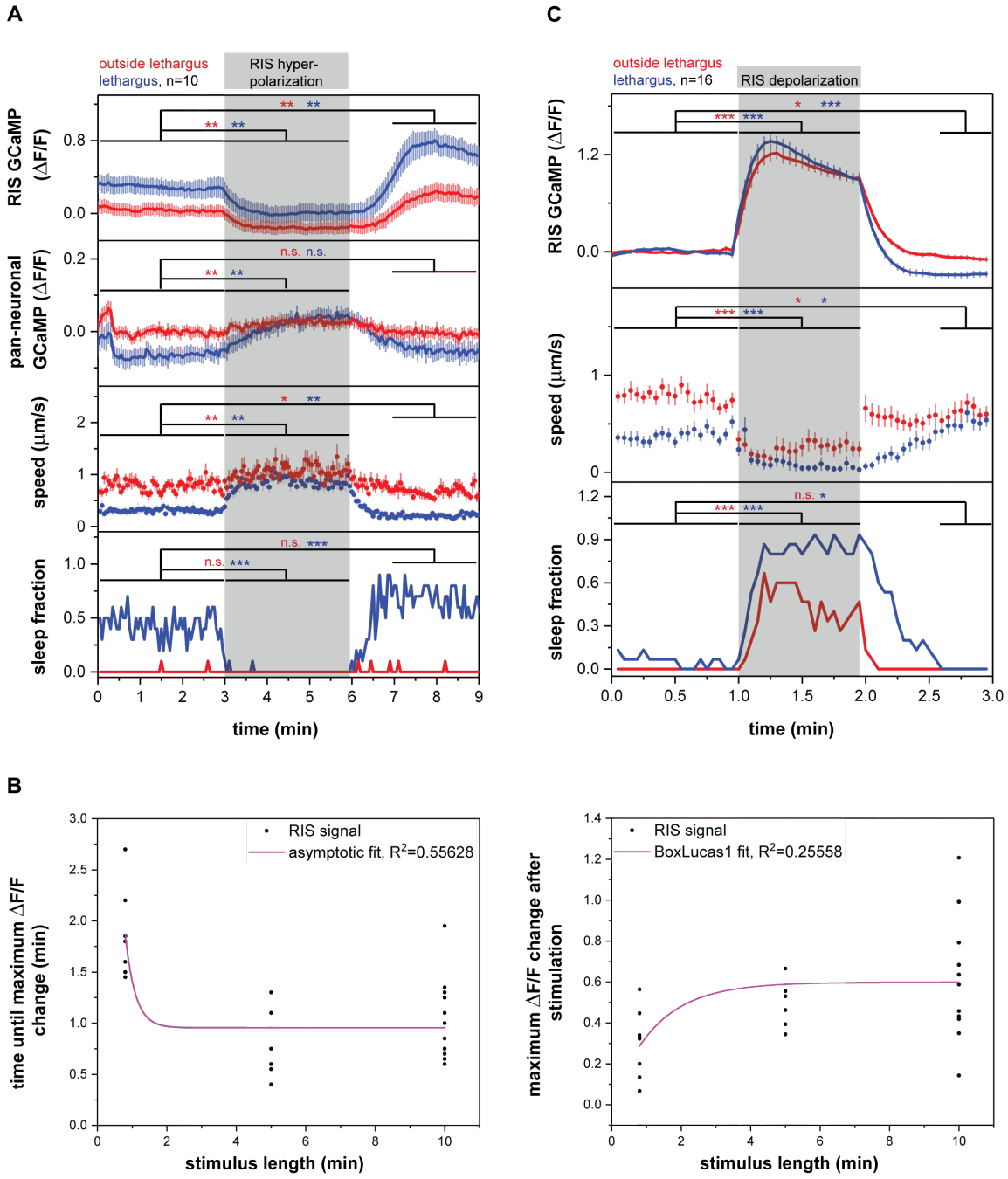
A
outside lethargus
lethargus, n=10
RIS hyper-polarization
RIS GCaMP (ΔF/F)
pan-neuronal GCaMP (ΔF/F)
speed (μm/s)
sleep fraction
time (min)
C
outside lethargus
lethargus, n=16
RIS depolarization
RIS GCaMP (ΔF/F)
speed (μm/s)
sleep fraction
time (min)
B
RIS signal
asymptotic fit, R²=0.55628
time until maximum ΔF/F change (min)
stimulus length (min)
RIS signal
BoxLucas1 fit, R²=0.25558
maximum ΔF/F change after stimulation
stimulus length (min)

1329 **Figure 3**

1330 **RIS depolarization is homeostatically controlled**

1331 A) RIS shows rebound activation following hyperpolarization. Behavioral and brain
1332 activity measurements correlate throughout the whole experiment; *$p < 0.05$, **p
1333 < 0.01, ***$p < 0.001$, Wilcoxon Signed Rank Test for GCaMP and speed,
1334 Fisher's Exact Test for sleep fraction.

1335 B) Dose-response curve of optogenetic RIS hyperpolarization with different stimulus
1336 lengths. RIS activation rebound transients saturate with increasing length of
1337 inhibition. Worms not showing a rebound activation transient after RIS
1338 optogenetic hyperpolarization were excluded from the analysis.

1339 C) RIS shows a negative rebound following its optogenetic depolarization; *$p < 0.05$,
1340 **$p < 0.01$, ***$p < 0.001$, Wilcoxon Signed Rank Test for GCaMP and speed,
1341 Fisher's Exact Test for sleep fraction.

1342

1343 **Figure 4**

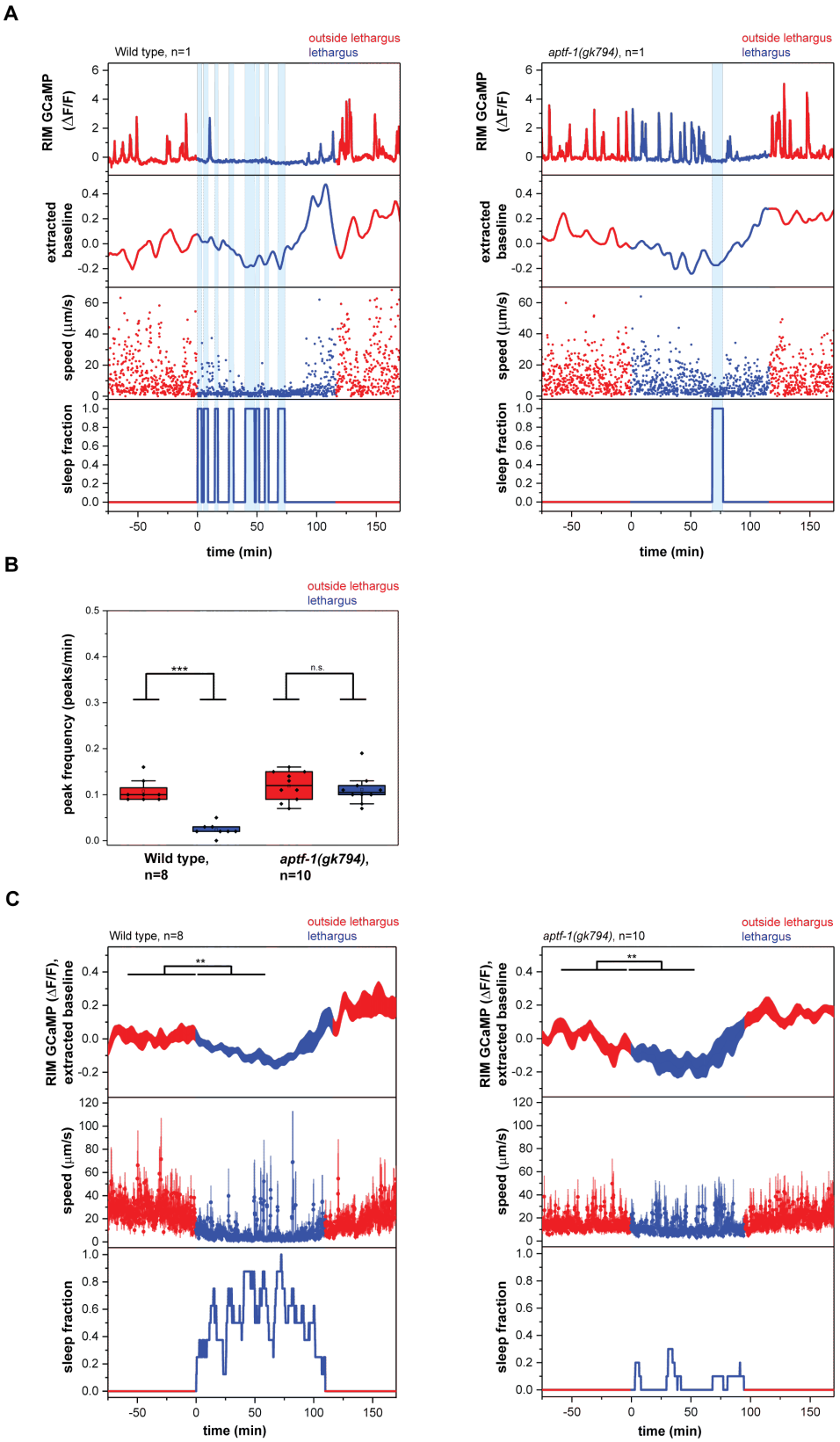

1344

1345 **Figure 4**

1346 **RIM activity levels are dampened in lethargus independently of RIS**

1347 A) Sample traces of RIM transient frequencies, RIM baseline activities and worm
1348 locomotion behaviors outside of and in lethargus in wild-type worms and *aptf-*
1349 *1(gk794)* mutants.

1350 B) Wild type worms, but not *aptf-1(gk974)* mutants display changes in RIM transient
1351 frequencies across lethargus. Transient frequencies were assessed manually. To
1352 be counted as a transient, RIM activity levels had to be at least twice as high as
1353 baseline activity levels. ***$p < 0.001$ Kolmogorov-Smirnov-Test for wild-type
1354 condition, Welch Test for mutant condition.

1355 C) The reduction of RIM baseline activity levels in lethargus is preserved in *aptf-*
1356 *1(gk974)* mutants; **$p < 0.01$, Wilcoxon Signed Rank Test.

1357

1358 **Figure 5**

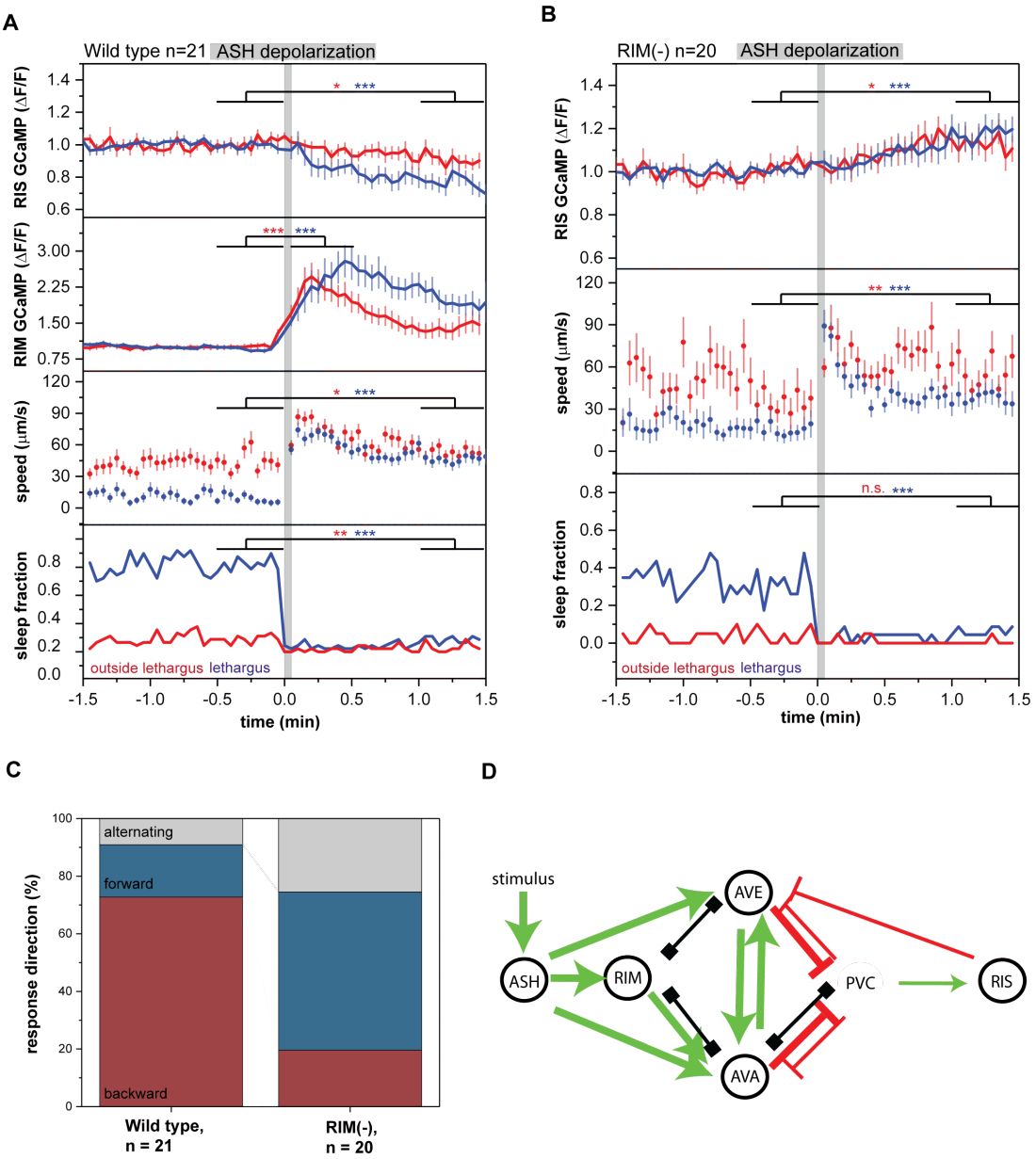

1359

1360 **Figure 5**

1361 **Arousing stimulation inhibits RIS and sleep through RIM**

1362 A) ASH depolarization in wild-type *C. elegans* leads to mobilization, awakening and
1363 RIS inhibition; *$p < 0.05$, **$p < 0.01$, ***$p < 0.001$, Wilcoxon Signed Rank Test
1364 for GCaMP and speed, Fisher's Exact Test for sleep fraction.

1365 B) ASH depolarization in RIM ablated *C. elegans* leads to weaker mobilization,
1366 awakening and RIS activation; *$p < 0.05$, **$p < 0.01$, ***$p < 0.001$, Wilcoxon
1367 Signed Rank Test for GCaMP and speed, Fisher's Exact Test for sleep fraction.

1368 C) The response direction following ASH activation in wild-type worms is
1369 predominantly backward, while in RIM ablated worms it is predominantly
1370 forward. This suggests that the forward direction is connected to RIS activation;
1371 ***$p < 0.001$, Fisher's Exact Test.

1372 D) A speculative circuit model for RIS regulation through arousal by ASH. RIM
1373 serves as synchronizer of AVE and AVA to regulate PVC and therefore RIS
1374 inhibition.

1375

1376 **Figure 6**

A) the circuit for sleep control in *C. elegans*

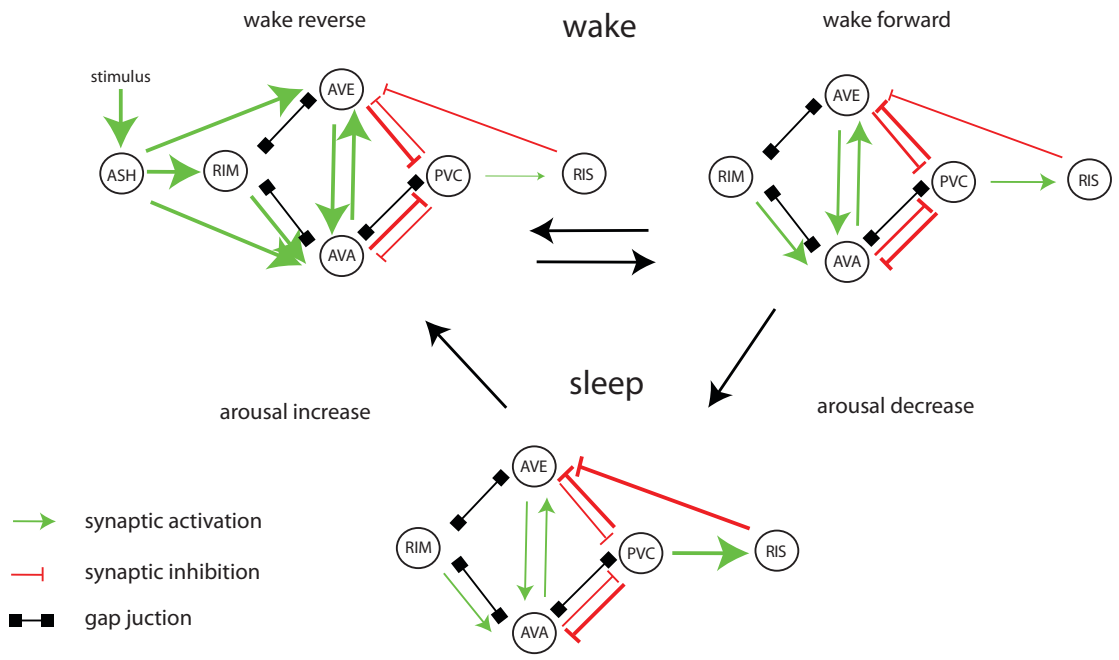

1377

1378 **Figure 6**

1379 **Model of the tripartite flip-flop sleep switch**

1380 A) Hypothetical model of the *C. elegans* sleep switch that is consistent with our data

1381 explaining the switch states.

1382 **Supplementary Information**

1383

1384 **Supplementary Figures**

1385

1386 **Figure S1**

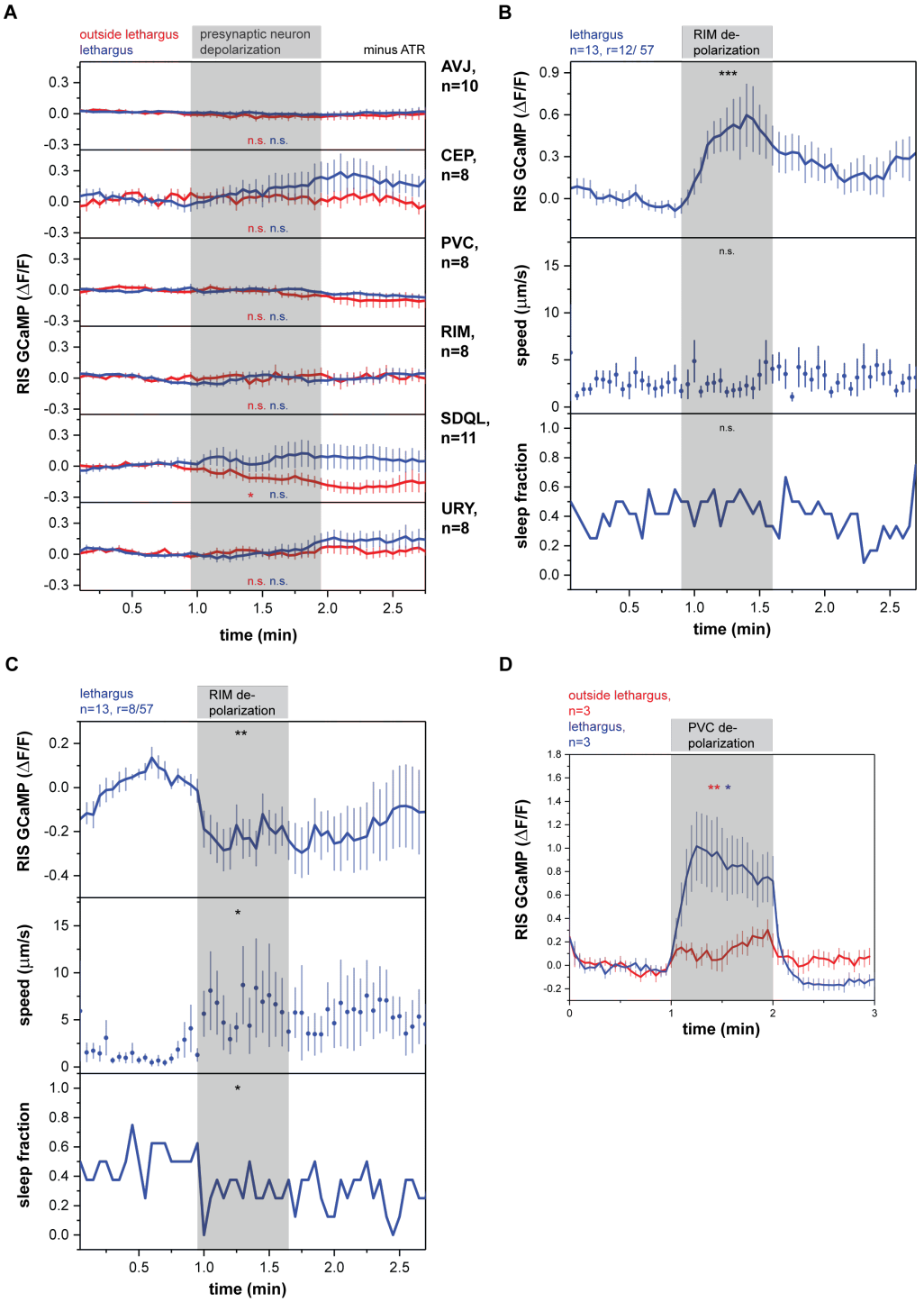

1387

1388

1389 **Figure S1**

1390 **RIM and PVC control RIS activity levels in lethargus**

1391 A) Control experiments. Optogenetic depolarization of RIS presynaptic neurons without
1392 the addition of ATR. For statistical calculations baseline neural activities (0 - 0.95 min)
1393 were compared to neural activity levels during the stimulation period (1 - 1.95 min); *p <
1394 0.05, compared before and during stimulation, Wilcoxon Signed Rank Test.

1395 B-C) RIM optogenetic depolarization can induce both RIS activation and inhibition.
1396 Single trials were classified as activating, if an activity increase in RIS correlated with
1397 onsets of optogenetic stimulation periods. Trials were classified as inhibitory, if an
1398 activity decrease in RIS correlated with onsets of optogenetic stimulation periods. n
1399 represents the number of animals tested, r represents the number of trials. For statistical
1400 testing baseline neural activities (0 - 0.95 min) were compared to neural activity levels
1401 during the stimulation period (1 - 1.55 min); *p < 0.05, **p < 0.01, ***p < 0.001,
1402 Wilcoxon Signed Rank Test for GCaMP and speed, Fisher's Exact Test for sleep
1403 fraction.

1404 D) Optogenetic PVC depolarization in L2 larvae leads to RIS activation outside of and in
1405 lethargus. RIS activation during lethargus is strongly enhanced. Plotted data represent the
1406 average over all experimental trials. Neural activity levels before the stimulation (0 - 0.95
1407 min) were compared to activity levels during the stimulation (1 - 1.95 min); *p < 0.05,
1408 **p < 0.01, Wilcoxon Signed Rank Test.

1409 **Figure S2**

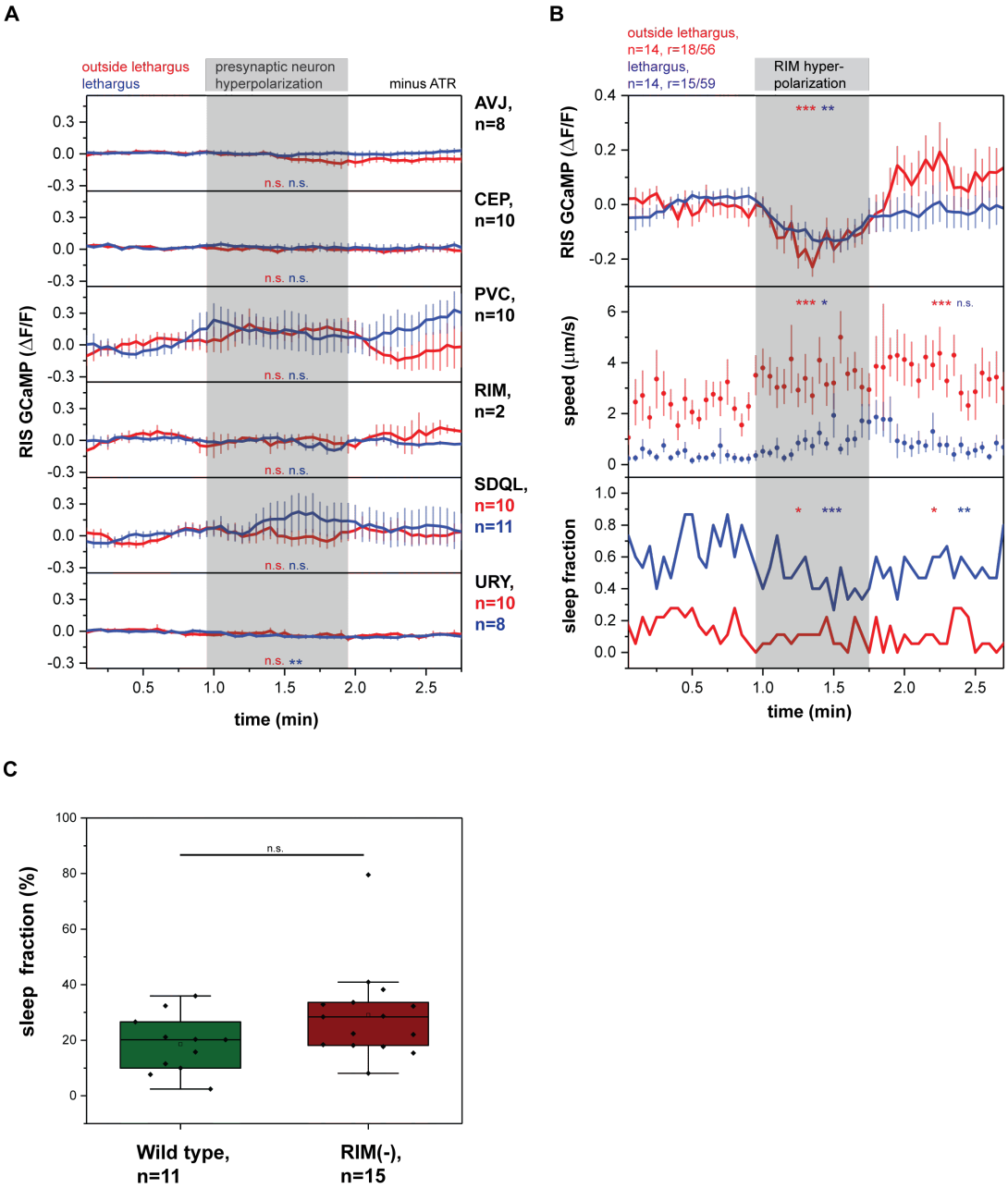

1410

1411 **Figure S2**

1412 **Hyperpolarization of RIS presynaptic neurons**

1413 A) Control experiments. Optogenetic hyperpolarization of RIS presynaptic neurons
1414 without the addition of ATR. Neural baseline activity levels (0 - 0.95 min) were
1415 compared to neuronal levels during the stimulation (1 - 1.95 min), except for experiments
1416 in which SDQL was stimulated. In these experiments the baseline was taken over the
1417 time interval of 0.6-0.95min; **$p<0.01$, Wilcoxon Signed Rank Test.

1418 B) RIM optogenetic hyperpolarization causes a decrease in RIS activity levels. Single
1419 trials were classified as activating, if an activity increase in RIS occurred at the onset of
1420 the optogenetic stimulation period. Trials were classified as inhibitory, if an activity
1421 decrease in RIS occurred at the onset of the optogenetic stimulation period. n represents
1422 the number of animals tested, r represents the number of trials. For statistical calculations
1423 neural baseline activity levels (0-0.95min) were compared to levels during the stimulation
1424 period (1-1.75min); *$p < 0.05$, **$p < 0.01$, ***$p < 0.001$, Wilcoxon Signed Rank Test for
1425 GCaMP and speed, Fisher's Exact Test for sleep fraction.

1426 C) RIM genetic ablation does not change spontaneous sleep amounts. n.s. $p > 0.05$.
1427 Kolmogorov-Smirnov-Test.

1428

1429 **Figure S3**

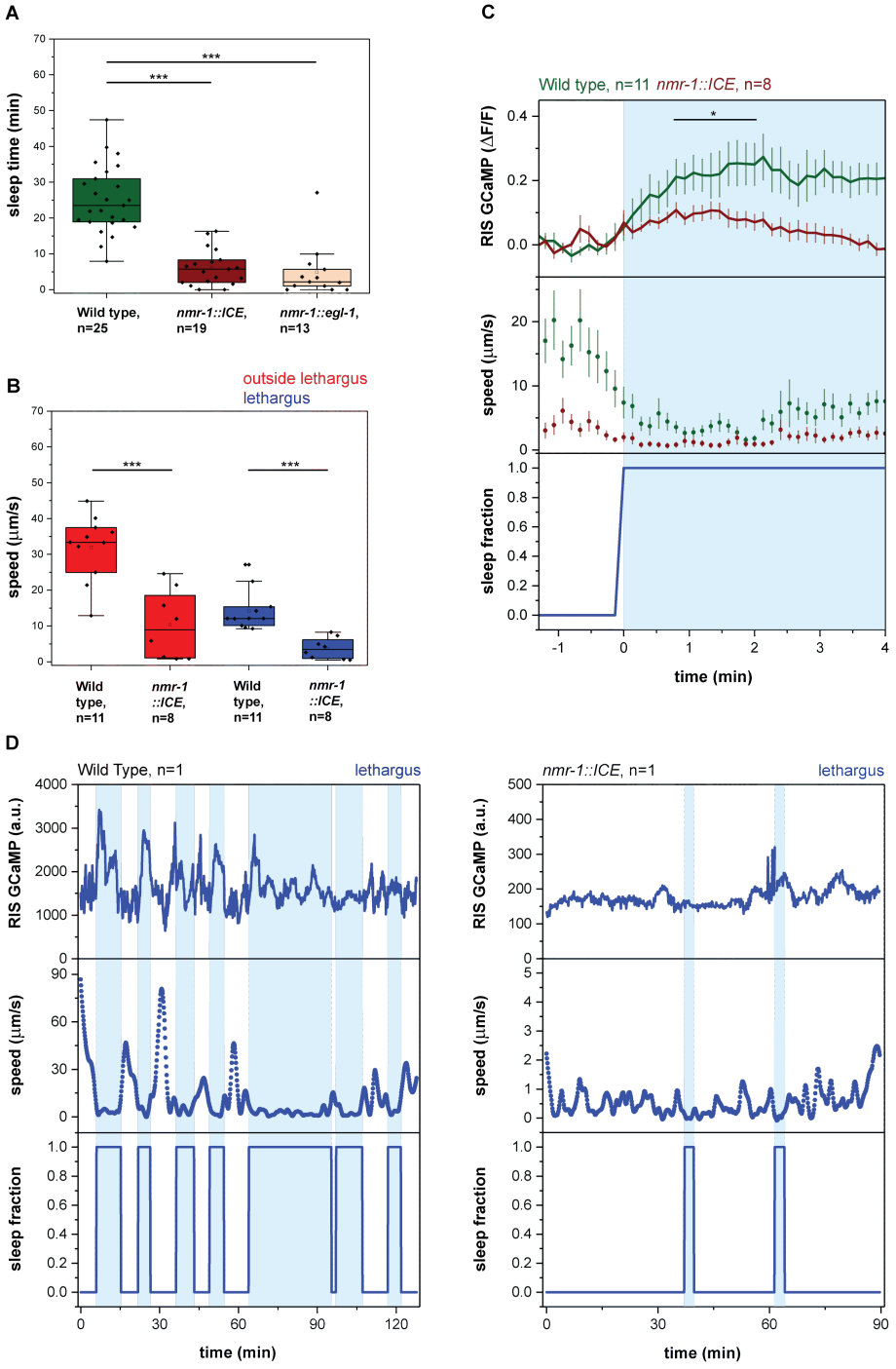

1430

1431 **Figure S3**

1432 **PVC and other command interneurons are required for sleep induction.**

1433 A) Genetic ablation of PVC and other command interneurons via expression of *ICE* or
1434 *egl-1* strongly reduced the occurrence of sleep bouts in lethargus. ***$p < 0.001$, Welch
1435 Test.

1436 B) PVC and other command interneuron ablated worms move much slower than wild-
1437 type worms. ***$p < 0.001$, Welch Test for the wake condition and Kolmogorov-
1438 Smirnov-Test for the sleep condition.

1439 C) RIS activation in sleep bouts is strongly reduced in PVC and other command
1440 interneuron ablated worms compared to wild-type worms. *$p < 0.05$, Welch Test.

1441 D) Sample traces of RIS activity levels and worm locomotion behaviors outside of and in
1442 lethargus in PVC and other command interneurons ablated worms and wild-type worms.
1443 In PVC and other command interneurons ablated worms sleep bouts occur only around
1444 the middle of the lethargus period.

1445 **Figure S4**

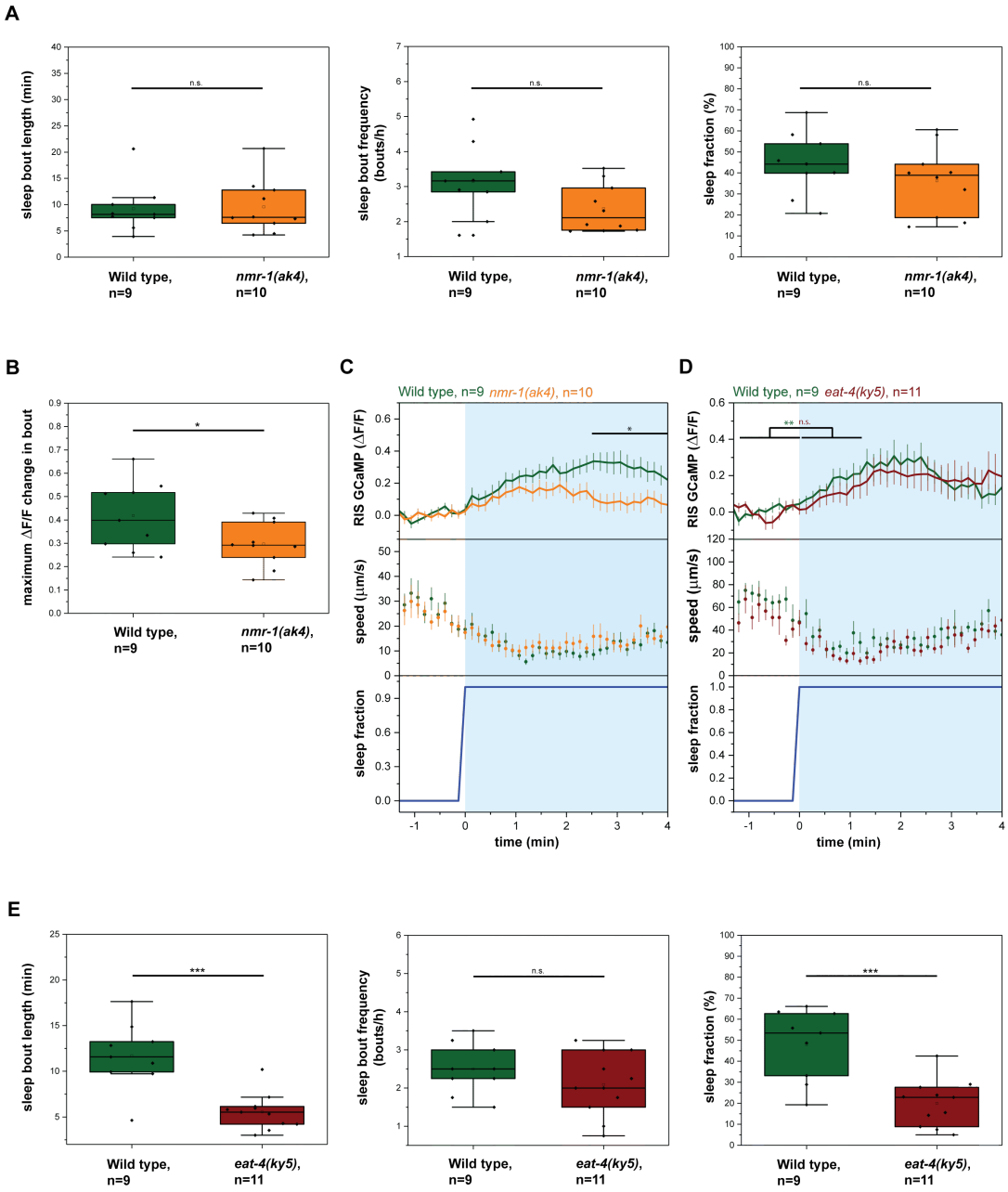

1446

1447

1448 **Figure S4**

1449 **Glutamatergic signaling is required for sleep induction**

1450 A-C) Sleep bout analysis of *nmr-1(ak4)* mutants. RIS activity levels in sleep bouts are
1451 reduced in the mutant background. Because RIS still activates in sleep bouts, *nmr-1(ak4)*
1452 mutants do not show a reduced amount of quiescence in lethargus. *$p < 0.05$, Welch Test
1453 for comparisons of sleep bout frequencies, sleep fractions, maximum RIS activity levels
1454 in sleep bouts and RIS activity levels at the end of sleep bouts. Kolmogorov-Smirnov-
1455 Test for the comparison of sleep bout lengths.

1456 D-E) Sleep bout analysis of *eat-4(ky5)* mutants. *eat-4(ky5)* mutants lack a significant RIS
1457 activation at sleep bout onsets. Consequently, mutants display a strong reduction in
1458 quiescence during lethargus. **$p < 0.01$, ***$p < 0.001$, Welch Test for comparisons of
1459 sleep bout lengths, sleep bout frequencies and sleep fractions. Wilcoxon Signed Rank
1460 Test for quantifications of RIS activity levels in sleep bouts.

1461 **Figure S5**

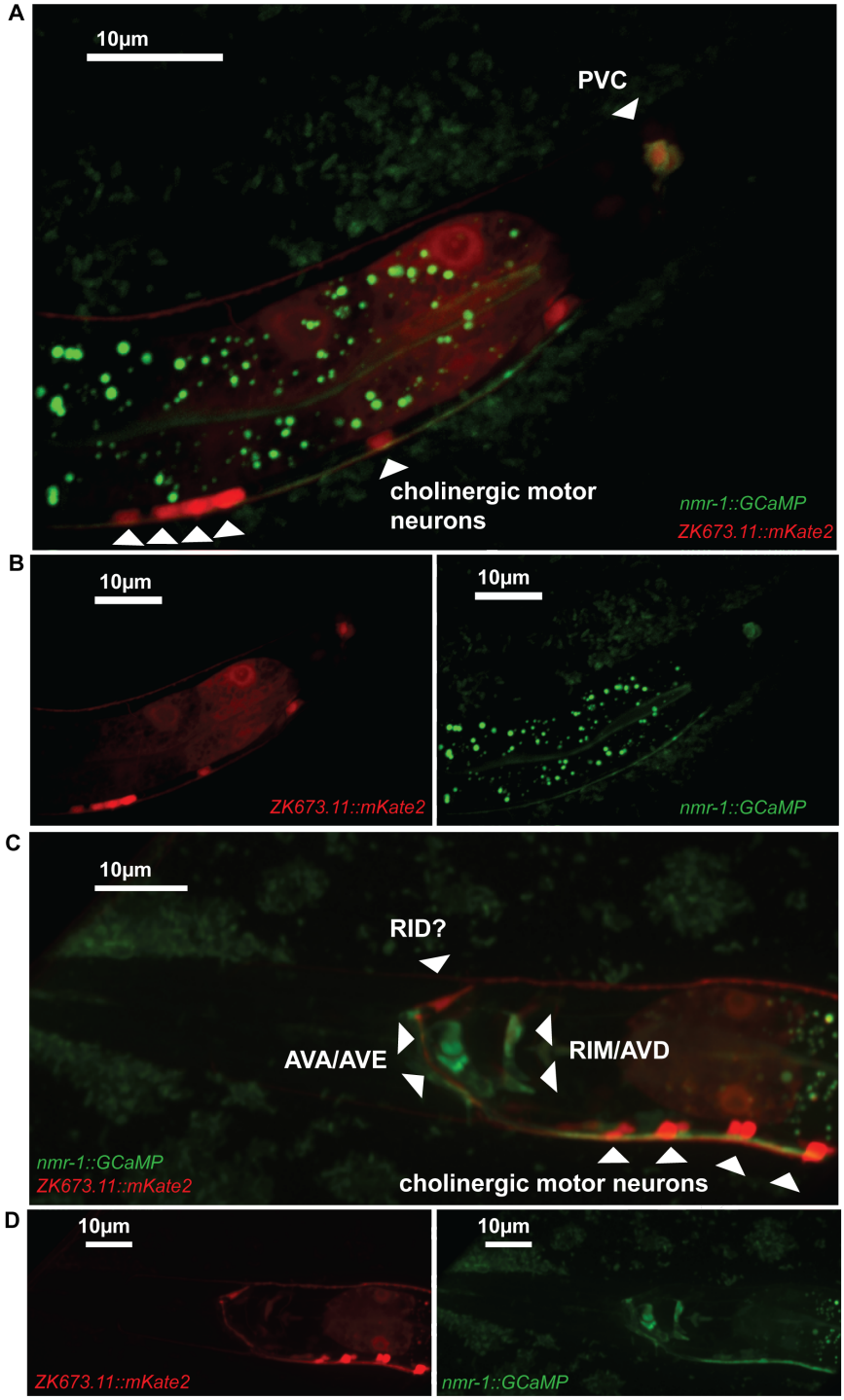

1462

1463 **Figure S5**

1464 ***ZK673.11* is expressed in PVC, RID and cholinergic motor neurons**

1465 A-B) Expression of *nmr-1* and *ZK673.11* only overlaps in PVC in the tail.

1466 C-D) Expression of *nmr-1* and *ZK673.11* does not overlap in head neurons.

1467 **Figure S6**

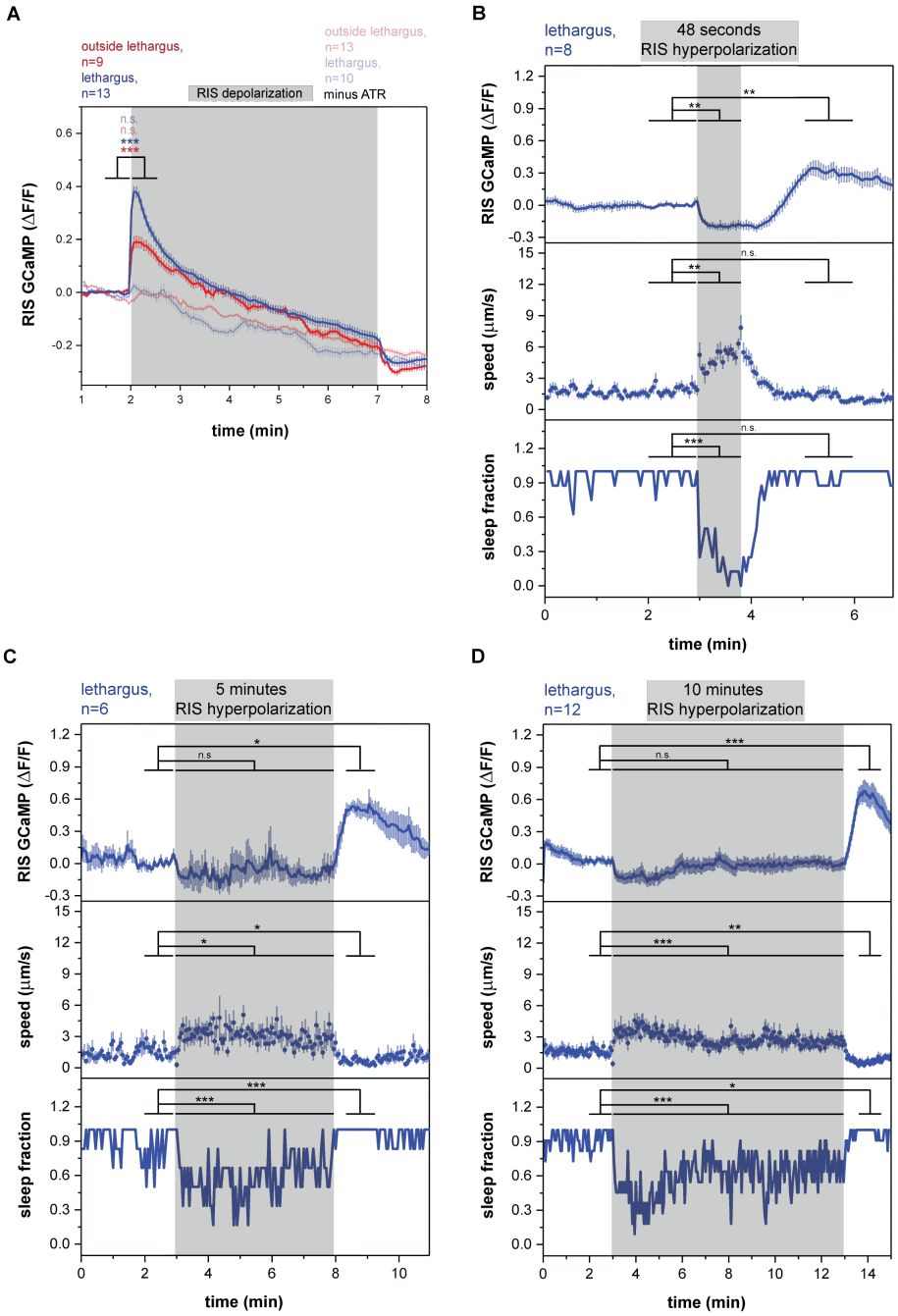

1468

1469 **Figure S6**

1470 **RIS rebound activation transients represent an acute phenomenon**

1471 A) RIS depolarizes during optogenetic activation in fixed animals. Experiments were
1472 repeated a second time without the addition of ATR. ***$p < 0.001$, Wilcoxon Signed
1473 Rank Test.

1474 B-D) RIS was optogenetically hyperpolarized with stimuli lasting for 48 seconds, 5
1475 minutes or 10 minutes. Worms not showing a rebound activation transient were excluded
1476 from the analysis. Data from these plots were used to generate a dose-response curve of
1477 optogenetic RIS hyperpolarization (Figure 3B). *$p < 0.05$, **$p < 0.01$, ***$p < 0.001$,
1478 Wilcoxon Signed Rank Test for GCaMP and speed, Fisher's Exact Test for sleep
1479 fraction.

1480

1481 **Figure S7**

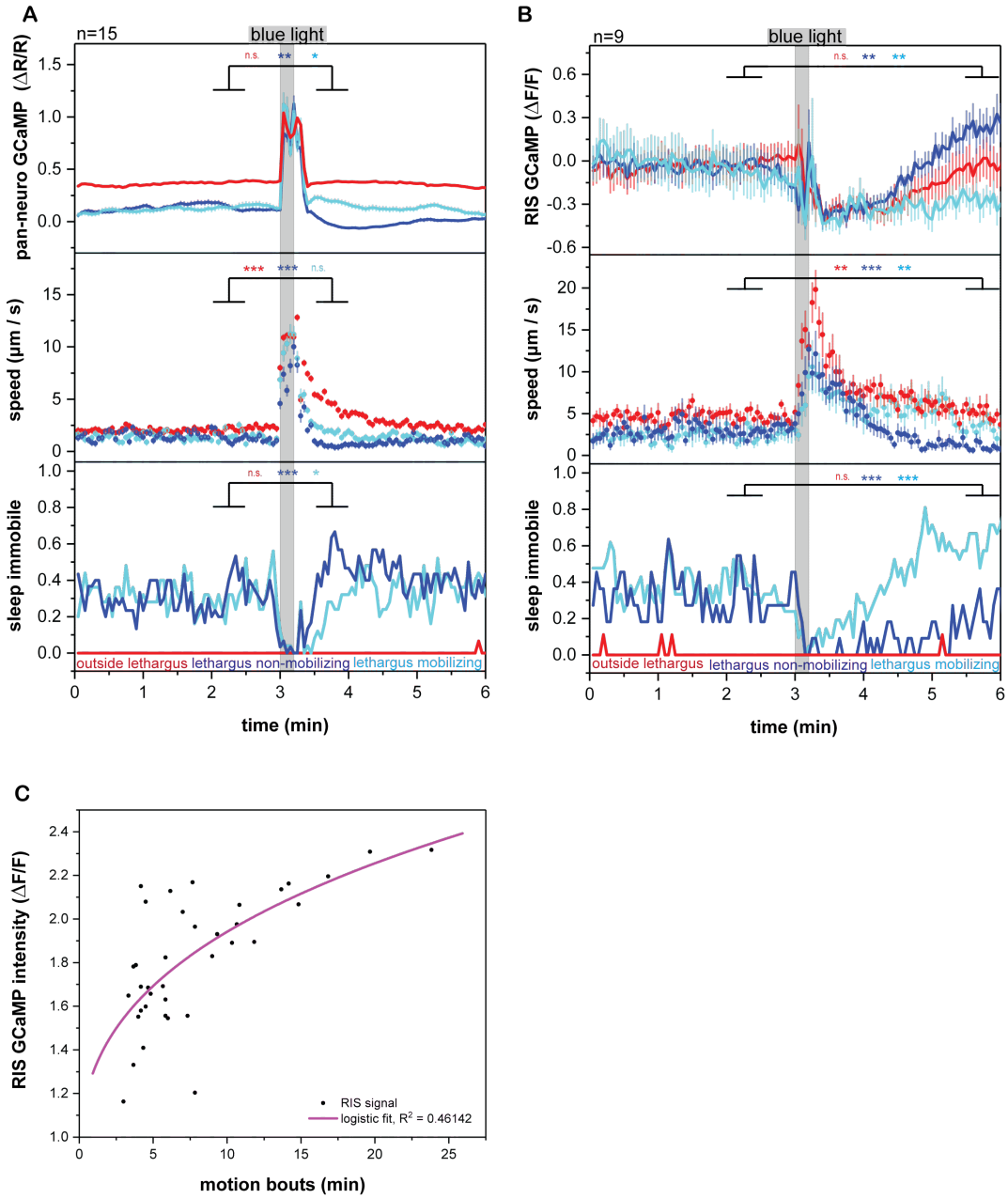

1482

1483

1484 **Figure S7**

1485 **RIS is homeostatically regulated**

1486 A-B) A blue light stimulus leads to awakening and mobilization of *C. elegans.* Worms
1487 that go back to sleep after the stimulus show a rebound: pan-neuronal inhibition below
1488 baseline levels and RIS activation above baseline levels; *$p < 0.05$, **$p < 0.01$, ***$p <$
1489 0.001, Wilcoxon Signed Rank Test for GCaMP and speed, Fisher's Exact Test for sleep
1490 fraction.

1491 A) The peak RIS GCaMP intensities in wild-type worms are homeostatically regulated by
1492 the preceding motion bouts. The longer the preceding motion bout, the stronger the RIS
1493 activation.

1494

1495 **Figure S8**

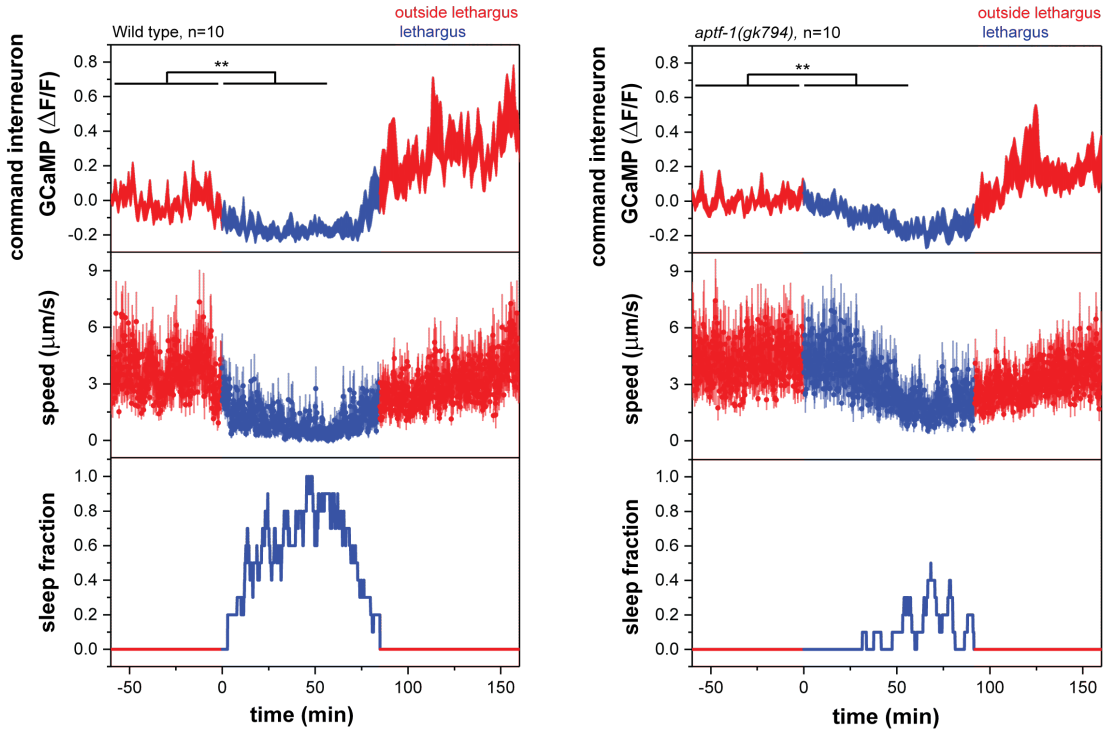

1496

1497

1498 **Figure S8**

1499 **The dampening of neural and behavioral baseline activity levels during lethargus is**

1500 **RIS-independent**

1501 Reduction of command interneuron activity levels in lethargus occurs in wild-type worms

1502 and *aptf-1(gk974)* mutants. In the wild-type condition activity levels are reduced to -0.16

1503 ± 0.02. In the mutant condition activity levels are reduced -0.08 ± 0.02. **$p < 0.01$,

1504 Wilcoxon Signed Rank Test.

1505

1506 **Figure S9**

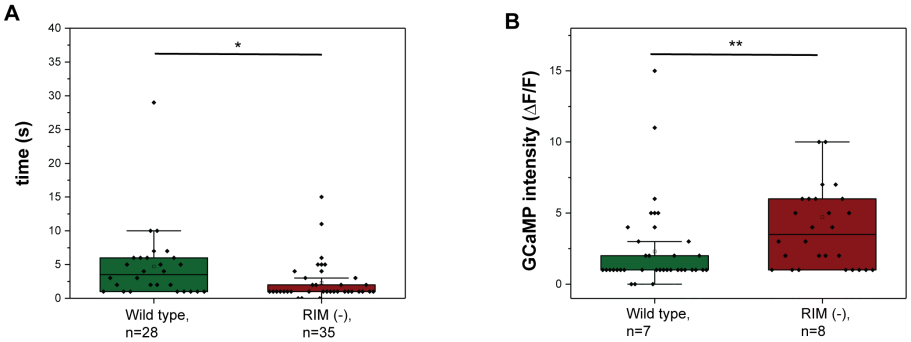

1507

1508

1509 **Figure S9**

1510 **Gentle tail touch reveals an inhibitory role of RIM on RIS**

1511 A) RIM ablation increases the reinstating of immobility following gentle tail touch during

1512 lethargus. *$p < 0.05$. Kolmogorov-Smirnov-Test.

1513 B) RIM ablation increases RIS activation in response to gentle tail touch. **$p < 0.01$.

1514 Kolmogorov-Smirnov-Test.

1515

1516

1517 **Supplementary Table**

1518

1519 **Table S1: Description of conditions used for optogenetics experiments**

Figure	Optogenetic Manipulation		Age	Mobile (m)/ Immobile (i)	ATR mM	Light Intensity mW/mm^2		Protocol				
	Genetic Tool	Neuron				490nm	585nm	Cycles	Delay	base-line	stimu-lation	reco-very
1B	tol-1:: ReaChR	URY	L1	m	50	0.33	0.37	15min	-	1min	1min	1min
	lad-2:: ReaChR	SDQL	L4	i	0.5	0.05	0.04	4	2min	1min	1min	1min
	gcy-13:: ReaChR	RIM	L1	m	50	0.33	0.37	30min	-	1min	1min	1min
	nmr-1:: ReaChR	PVC	L1	i	50	0.05	0.26	1	5min	2min	1min	2min
	dat-1:: ReaChR	CEP	L4	m	0.5	0.14	0.09	30min	-	1min	1min	1min
	hlh-34:: ReaChR	AVJ	L1	m	50	0.33	0.37	15min	-	1min	1min	1min
1C	tol-1:: ArchT	URY	L4	m	0.5	0.11	0.39	30min	-	3min	3min	8min
	lad-2:: ArchT	SDQL	L4	i	0.5	0.05	0.09	4	5min	1min	1min	1min
	gcy-13:: ArchT	RIM	L1	m	50	0.33	0.37	30min	-	1min	1min	1min
	nmr-1:: ArchT	PVC	L1	i	50	0.12	0.26	1	5min	2min	1min	2min
	dat-1:: ArchT	CEP	L1	m	50	0.33	0.17	15min	-	1min	1min	1min
	hlh-34:: ArchT	AVJ	L1	m	50	0.33	0.37	15min	-	1min	1min	1min
1D	ZK673.11 ::ArchT	PVC	L1	m	10	0.07	0.17	20min	-	2min	1min	3min
2B	flp-11:: ReaChR	RIS	L1	i	10	0.28	3.39	2	1min	2min	5min	1min
2C	flp-11:: ArchT	RIS	L1	i	10	0.05	0.09	2	1min	1min	1min	1min
3A	flp-11:: ArchT	RIS	L1	m	50	0.07	0.17	30min	-	3min	3min	8min
3B, S6	flp-11:: ArchT	RIS	L1	m	50	0.15	0.17	15min	-	1min	48s	1min
	flp-11:: ArchT	RIS	L1	m	50	0.15	0.17	15min	-	3min	5min	3min
	flp-11:: ArchT	RIS	L1	m	50	0.1	0.17	15min	-	3min	10min	3min
3C	flp-11:: ReaChR	RIS	L1	m	50	0.15	0.09	15min	-	1min	1min	1min
5A	sra-6:: ReaChR	ASH	L4	m	0.2	0.6	0.14	15min	-	1.5min	3s	87s
5B	sra-6:: ReaChR	ASH	L4	m	0.2	0.6	0.14	15min	-	1.5min	3s	87s
S1A,B	gcy-13:: ReaChR	RIM	L1	m	50	0.33	0.37	30min	-	1min	1min	1min
S1C	gcy-13:: ArchT	RIM	L1	m	50	0.33	0.37	30min	-	1min	1min	1min
S1D	nmr-1:: ReaChR	PVC	L2	i	50	0.05	0.01	2-3	-	1min	1min	1min
S5A	tol-1:: ReaChR	URY	L1	m	0	0.33	0.37	15min	-	1min	1min	1min
	lad-2:: ReaChR	SDQL	L4	i	0	0.05	0.04	4	2min	1min	1min	1min

Table S1. Optogenetic Experimental Details.